A Multi-stage inversion framework for dynamic fracture characterization and long-term thermal performance prediction in an Enhanced Geothermal System

Kun Zhang[1], Hui Wu[1, 2*]

[1] School of Earth and Space Sciences, Peking University, Beijing, China.

[2] Peking University Ordos Research Institute of Energy, Ordos, 017010, China.

Corresponding author: Hui Wu (hui.wu@pku.edu.cn)

Key Points:

- A multi-stage inversion framework integrating data assimilation with thermo-hydro-mechanical model for dynamic fracture characterization.
- Application to a field-scale model demonstrates an improved thermal prediction accuracy compared with previous single-stage inversion.
- Effect of inversion timing on aperture inversion and thermal prediction is analyzed to provide implications for real-world applications.

Abstract

Fractures play important roles in fluid and heat flow during heat extraction from an enhanced geothermal system (EGS). Quantifying the associated uncertainties in fractures is critical for predicting long-term thermal performance of EGSs. Considerable advancements have been made regarding the inversion of fracture characteristics such as aperture distribution. However, most previous studies assumed a constant fracture aperture to simplify the inversion, while both experimental and numerical results indicated significant variations in fracture aperture due to complex thermo-hydro-mechanical (THM) coupled processes during heat extraction. This study introduces a multi-stage inversion framework that integrates the Ensemble Smoother with Multiple Data Assimilation (ES-MDA) with a THM coupled model to capture the dynamic evolution of fracture aperture. The framework executes multiple aperture inversions at different times during EGS operation. In each inversion stage, we use ES-MDA to invert for fracture aperture by assimilating tracer data, and then perform THM modeling to analyze fracture aperture evolution under coupled THM processes and predict thermal performance. We propose a principle to assure a smooth transition between two consecutive inversion stages, that the posterior aperture fields obtained in an inversion stage are used as the prior aperture fields for the following stage, and the temperature field simulated in the previous inversion stage serves as the initial temperature field for the following stage. Application of the framework to a synthetic field-scale EGS model demonstrates its efficacy in capturing the dynamic evolution of fracture aperture, resulting in more accurate thermal predictions compared with previous inversion methods assuming constant fracture aperture.

Plain Language Summary

Enhanced geothermal systems (EGS) generally rely on artificial and/or natural fractures as pathways for fluid circulation (typically water) and heat transfer to extract heat from hot dry rocks. Due to the deep geological location, directly observing and measuring fracture characteristics is rather difficult, if not impossible. Researchers typically use geophysical and hydrological data to indirectly infer fracture characteristics. However, previous studies mostly speculated only on the initial fracture characteristics in an EGS, neglecting or being unable to capture dynamic changes in fractures during heat production, inevitably leading to biased long-term thermal prediction. We propose a multi-stage inversion framework that estimates the distribution of fracture apertures at different stages of EGS operation. This allows us to continuously and accurately capture changes in fracture aperture caused by coupled thermo-hydro-mechanical (THM) processes. In this framework, we use an ensemble smoother to infer fracture aperture distributions from tracer test data, along with a specialized computer code to simulate the coupled THM processes for thermal prediction. Examining this framework on a synthetic field-scale EGS model shows more accurate thermal performance predictions compared with traditional inversion methods. Accurate thermal predictions are beneficial for better planning for geothermal energy utilization and effective risk management.

1 Introduction

The increasing global demand for sustainable and clean energy resources has driven the exploration and development of various innovative energy technologies. Among these technologies, enhanced geothermal systems (EGS) are considered promising in improving the current global energy consumption structure due to their ability to extract heat from hot dry rocks that contain abundant renewable geothermal resources (Li et al., 2022; Olasolo et al., 2016;

Tester et al., 2007). In EGS development, the accurate estimation of long-term thermal performance is essential for the optimization of engineering decisions and risk management (Wu et al., 2021a). As hot dry rocks largely reserve at several kilometers below the ground surface, the development of an EGS generally encounters complex geological conditions that are rather difficult to measure/observe directly. Important information on subsurface properties, such as matrix permeability, fracture distribution and fracture aperture field, is often quite limited, leading to a high level of uncertainties in EGS development (Liu et al., 2018; Pollack & Mukerji, 2019; Vogt et al., 2012; Witter et al., 2019). These uncertainties impede a comprehensive understanding of fluid circulation and heat transfer processes within an EGS reservoir, thus posing a significant challenge to the thermal performance estimation of the EGS.

In recent decades, substantial efforts have been dedicated to developing inversion methods to resolve subsurface uncertainties and improve the prediction capability of EGS thermal performance. For an EGS reservoir, a major uncertainty associated with fluid flow and thermal transport processes is fracture characteristics as fractures are primary fluid flow paths during heat extraction. Widely used fracture inversion algorithms involve stochastic approaches (Jiang et al., 2023; Ringel et al., 2021; Somogyvári et al., 2017; Wu et al., 2021b), deep learning methods (Chandna & Srinivasan, 2022; Jiang et al., 2021; Vu & Jardani, 2022) and ensemble-based data assimilation (Elahi & Jafarpour, 2018; Liem et al., 2022; Liem & Jenny, 2020; Ping & Zhang, 2013; Wu et al., 2021a). Amongst, ensemble-based methods are considered computationally more efficient and enable an easy integration with forward models for inverse problems. The variability among ensemble-based realizations can represent uncertainties arising from different sources. The inversion of fracture characteristics also heavily relies on the quality and quantity of available geological, geophysical and hydrological data such as seismic and electrical data, hydraulic and tracer testing data, etc. (Berkowitz, 2002; Ren et al., 2023; Tarrahi et al., 2015; Wu et al., 2019, 2021b). Previous research indicates that microseismic data enables the identification of fracture networks in EGS reservoir (Tarrahi et al., 2015), while tracer data can effectively inform hydraulic characteristics of reservoirs and provides key information about fracture aperture and distribution (Egert et al., 2020; Elahi & Jafarpour, 2018; Liu et al., 2023; Ren et al., 2023; Wu et al., 2021a). Interwell tracer test have been applied in conventional/unconventional reservoirs for decades, demonstrating its effectiveness in reservoir characterization (Abbaszadeh-Dehghani & Brigham, 1984; Chen et al., 2022; Shook & Suzuki, 2017). Our previous work successfully developed a data assimilation framework to interpret tracer test data, facilitating the inversion of the fracture aperture distribution in an EGS (Wu et al., 2021a). With the inversion framework, predicting long-term thermal performance of a sing-fracture EGS under constant fracture properties has been properly addressed.

A significant challenge associated with EGS fracture characterization is that fracture aperture/permeability dynamically evolves due to the coupled hydro-thermal-mechanical-chemical processes rather than remains constant during the production lifetime of an EGS. For example, thermal drawdown-induced thermal stress has been recognized as a major mechanism for fracture aperture evolution. The thermal stress can reduce the effective compressive stress that acts on the fractural flow pathways and therefore increases the apertures of fracture. As an EGS mainly relies on fractures for fluid flow and heat transfer, the influence of thermal stress on fracture characteristics is critical for heat production from the EGS. In fact, thermal stress has proven a main cause of flow channeling (or short-circuiting), a widely recognized phenomenon that fluid concentrates in several preferential flow channels between injection and production wells (Fu et al., 2016; Gee et al., 2021; Ghassemi & Suresh Kumar, 2007; Guo et al., 2016;

McLean & Espinoza, 2023; Vik et al., 2018). As a result of flow channeling, effective heat exchange area between fracture fluid and adjacent rock formations is reduced and heat recovery is impaired. Guo et al. (2016) conducted a comprehensive investigation on the effect of thermal stress through a single-fracture EGS model. They concluded that thermal stress could lead to premature thermal breakthrough, and ignoring the influence of thermal stress might overestimate the EGS lifespan by more than 20 years. In addition, chemical reactions (dissolution and precipitation) constitute another crucial mechanism for the dynamic evolution of fracture characteristics (Detwiler, 2008; Pandey et al., 2014; Salimzadeh & Nick, 2019; Song et al., 2022; Yasuhara et al., 2011). Dissolution may lead to an increase in fracture aperture, while precipitation typically leads to a reduction in aperture.

Unfortunately, most previous studies ignored the dynamic evolution of fracture aperture while performing fracture inversion and thermal prediction for EGSs. In other words, only the initial fracture aperture was inverted for and used for subsequent analyses such as thermal performance prediction. Although Wu et al. (2021a) proposed an effective tracer data interpretation framework for fracture aperture inversion in a single-fracture EGS model, they adopted a thermo-hydraulic (TH) model for thermal simulation, thus did not consider fracture aperture evolution due to thermal stress. The inferred aperture distribution was assumed to remain constant during the lifetime of the EGS model. As aforementioned, the thermal drawdown-induced thermal stress may cause significant changes in fracture aperture and further affect long-term thermal performance. Directly using the initially inferred fracture aperture distribution for flow and thermal modeling inevitably leads to biased thermal predictions. To improve the inversion accuracy and provide a reliable thermal prediction for engineering decision making, both the initial fracture aperture distribution and its dynamic evolution during heat extraction should be appropriately characterized through advanced inversion strategies.

In this study, we propose a multi-stage data assimilation framework for the inversion of fracture aperture from tracer data and capture the dynamic evolution of aperture distribution during the lifetime of EGSs. The proposed framework extends the framework in Wu et al. (2021a) by integrating a thermo-hydro-mechanical (THM) coupled model to account for the thermal stress effect and incorporates multi-stage fracture inversions. Each inversion stage uses the posterior aperture ensemble from the previous inversion stage as the prior ensemble, ensuring a progressive refinement of the inversion model rather than a random modification. The key novelty of our study is to dynamically characterize fracture aperture evolution through multi-stage inversion to gradually improve the accuracy of long-term thermal prediction of EGSs.

The remainder of the paper is organized as follows. Section 2 briefly describes the major components of the proposed framework. Section 3 introduces a synthetic field-scale EGS model for subsequent verification of the proposed framework. In Section 4, we apply the proposed framework to the EGS model and investigates the effectiveness of the framework in capturing dynamic fracture aperture evolution and thermal performance prediction. Section 5 provides discussions and implications regarding the application of the proposed framework.

2 Multi-stage inversion strategy

As mentioned before, although the framework proposed by Wu et al. (2021a) is capable of fracture aperture inversion and thermal prediction, it assumes a constant aperture distribution and therefore is unable to capture the dynamic evolution of fracture aperture during heat extraction. To address this issue, we propose a multi-stage inversion strategy based on the framework from Wu et al. (2021a) (Figure 1). The key of the strategy is to perform multiple aperture inversions using tracer data obtained at different times during EGS operation, and thus, dynamically update fracture aperture distribution to improve thermal prediction accuracy. Compared with many previous studies that only performed a onetime aperture inversion (e.g., Elahi and Jafarpour, 2018; Liem et al., 2022; Liem and Jenny, 2020; Wu et al., 2021), the present study aims to invert for fracture aperture multiple times to obtain snapshots of aperture field during the lifetime of an EGS. The rationale and technical feasibility of such a multi-stage inversion is that tracer testing can be performed repeatedly during fluid circulation in EGS reservoirs with relatively low cost. Since the time required to complete a tracer testing (days to months) is much shorter than the lifespan of an EGS (decades), the aperture field almost remains constant during the period of a tracer testing, and therefore the aperture inversion result can be considered a reasonable estimate of the aperture field at the time of this tracer testing.

In the following, we first briefly introduce the data assimilation framework from Wu et al. (2021a), and then describe the multi-stage inversion strategy for the inversion of dynamic aperture evolution.

2.1 A data assimilation framework for aperture inversion and thermal prediction

The data assimilation framework from Wu et al. (2021a) includes three major components: (1) Low-rank parameterization of fracture aperture; (2) Fracture aperture inversion through Ensemble Smoother with Multiple Data Assimilation (ES-MDA); (3) Thermal modeling and prediction based on the inverted apertures. A brief description of each component is given as follows.

2.1.1 Low-rank parameterization

A significant challenge in fracture aperture inversion is the ill-posedness issue arising from the inherent complexity of aperture distribution and the limited availability of measurements. Dimensionality reduction methods have been applied to map high-dimensional aperture fields to low-rank latent spaces, thus reduce the complexity of original aperture fields and accommodate the data scarcity issue. In the framework of Wu et al. (2021a), principal component analysis (PCA) was used for dimensionality reduction through a set of principal components that retain the most critical features of original aperture fields. These principal components can be obtained either by performing singular value decomposition (SVD) or calculating the eigenvectors and eigenvalues of the original aperture fields. The components are ranked based on their significance, with the higher-ranked components explaining higher variances in original aperture fields. By truncating less significant components, PCA allows to represent the original aperture fields in a more compact form. We refer to Wu et al. (2021a) for further information on the low-rank parameterization of fracture aperture fields with PCA.

2.1.2 ES-MDA inversion

The latent parameters obtained from PCA are then inverted for using ES-MDA, an ensemble smoother that repeatedly assimilates measurements with an expanded measurement error covariance matrix to iteratively estimate model parameters (Emerick and Reynolds, 2013). Without going into mathematical derivation details, we briefly overview the workflow of ES-MDA. Detailed information on ES-MDA algorithm can be found in the reference (Emerick & Reynolds, 2013; Evensen, 2018; Le et al., 2016; Ranazzi & Sampaio, 2019; Todaro et al., 2022).

ES-MDA begins with generating a prior ensemble of latent parameters with an ensemble size of N_e, denoted as $\mathbf{Z}^0 = \left[\mathbf{z}_1^0\ \mathbf{z}_2^0\ \ldots\ \mathbf{z}_{N_e}^0\right] \in \mathbb{R}^{l\times N_e}$, where l is the dimension of latent parameter. As the latent parameters obtained from PCA approach follow the standard normal distribution, the prior ensemble parameter $\mathbf{Z}^0$ is randomly sampled from $\mathcal{N}(0,1)$. With the prior parameter ensemble, ES-MDA then proceeds with iterative forecast and update steps.

At each iteration of ES-MDA, we first remap the latent parameters into aperture fields, and then perform tracer modeling with the aperture fields to forecast model responses $\mathbf{y}_j^i$ (tracer breakthrough data in this study, *i* denotes iteration index and *j* denotes realization number in the ensemble). In the update step, the ensemble of latent parameters is updated as follows,

$$\mathbf{z}_j^i = \mathbf{z}_j^{i-1} + \mathbf{C}_{\mathrm{ZY}}^{i-1}(\mathbf{C}_{\mathrm{YY}}^{i-1} + \alpha_i \mathbf{R})^{-1}(\mathbf{y}_{\mathrm{obs}} + \sqrt{\alpha_i}\boldsymbol{e}_j - \mathbf{y}_j^{i-1}) \tag{1}$$

where $\mathbf{C}_{\mathrm{ZY}}^{i-1} \in \mathbb{R}^{l\times N_d}$ denotes the cross-covariance matrix between the ensemble of parameters $\mathbf{Z}^{i-1}$ and its corresponding model predictions $\mathbf{y}^{i-1}$; $\mathbf{C}_{\mathrm{YY}}^{i-1} \in \mathbb{R}^{N_d\times N_d}$ denotes the auto-covariance matrix of predictions; $\mathbf{R} \in \mathbb{R}^{N_d\times N_d}$ denotes the auto-covariance matrix of the measurement errors of the observation data ($\mathbf{y}_{\mathrm{obs}}$) to be assimilated; ε_j is the measurement error following a Gaussian distribution $\mathcal{N}(0,\mathbf{R})$; α_i is the inflation factor at the current iteration that must satisfy $\sum_{i=1}^{N_a}\alpha_i^{-1} = 1$, where N_a denotes the total iteration number.

After the current update, the procedure continues to the next forecast and update steps until the final iteration is completed.

2.1.3 Thermal performance prediction

The third component of the framework from Wu et al. (2021a) is to perform thermal modeling and make long-term thermal performance predictions. The posterior ensemble of latent parameters obtained from ES-MDA is remapped to the posterior ensemble of fracture aperture fields, which is then incorporated into a thermo-hydraulic model for thermal modeling.

2.2 Multi-stage inversion strategy

The framework from Wu et al. (2021a) can be considered as a one-time inversion as ES-MDA is executed only once to characterize the initial fracture aperture distribution. To capture the dynamic evolution of fracture aperture during EGS heat recovery, the present study further extends the framework from Wu et al. (2021a) to a multi-stage inversion framework, which performs multiple tracer tests and fracture aperture inversions throughout the lifetime of the EGS (Figure 1). Such a framework dynamically updates fracture aperture based on new tracer data to accommodate the impacts of the mechanical and chemical influences on fracture aperture and flow fields.

The multi-stage framework consists of multiple consecutive inversion stages, with each stage refining model parameters based on insights obtained from previous inversion stages and new observations/measurements. For the initial stage, the prior ensemble is randomly generated from $\mathcal{N}(0,1)$ as aforementioned. For subsequent inversion stages, the posterior ensemble from the previous inversion is utilized as the prior ensemble. This approach capitalizes on the fact that the previous inversion has already reduced uncertainties in aperture distribution, thus providing a relatively reliable starting point for the subsequent inversion stage. Since tracer data is used as the major inversion data in the present study, a tracer testing is performed before each inversion stage to provide new measurements. Within each stage, the major inversion procedures are the same as that in Wu et al. (2021a), as illustrated in Section 2.1.

After the completion of each inversion stage, we incorporate the obtained posterior fracture aperture field into a thermo-hydro-mechanical model to perform THM coupled simulations for thermal performance prediction. Note that each time fracture aperture is updated, the simulated temperature field at the end of the previous THM simulation is utilized as the initial temperature field for the following THM simulation.

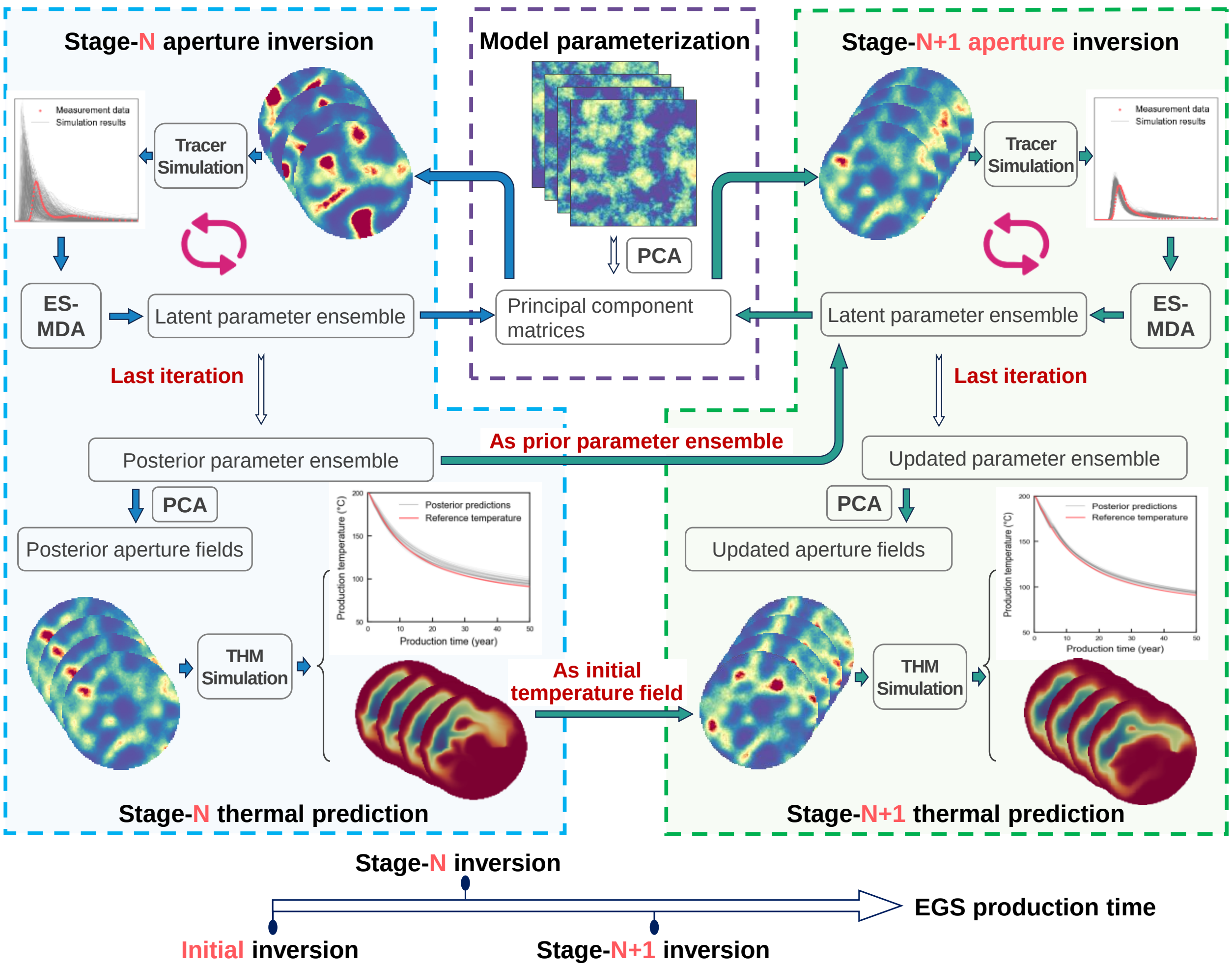

Figure 1. Multi-stage inversion framework to invert for the dynamic evolution of fracture aperture from tracer test data.

3 Numerical model

3.1 Model setup

In this section, we design a synthetic field-scale EGS model with a single fracture to examine the capability of the proposed multi-stage inversion framework in dynamic aperture inversion as well as long-term thermal forecasting. The EGS model spans dimensions of 3 km × 3 km × 3 km, and has one injection well and one production well connected by a horizontal circular fracture in a low-permeability rock formation (Figure 2). The diameter of the fracture is

1 km, and the distance between the injection and production wells is 600 m. The model is initially saturated with water, and exhibits a vertical geothermal gradient of 40 °C/km with an initial temperature of 200 °C at the depth of the fracture. We use an orthogonal grid to discretize the reservoir model. Specifically, the fracture is discretized with a thin layer of solid elements, each has a resolution of 10 m × 10 m × 4 mm, and the rock matrix elements adjacent to the fracture are sized at 10 m × 10 m × 1 cm. The mesh resolution gradually coarsens from the fracture to far field, maintaining a balance between computational costs and modeling accuracy.

To simulate the high heterogeneity of fracture aperture distribution, we design a procedure employing three different Gaussian distributions to create a fracture aperture field (Figure 2). First, the sequential gaussian simulation algorithm is applied to generate three 100 × 100 two-dimensional random Gaussian fields following $\mathcal{N}(0.6\ \text{mm},\ (0.7\ \text{mm})^2)$, $\mathcal{N}(0.4\ \text{mm},\ (0.5\ \text{mm})^2)$, $\mathcal{N}(0.8\ \text{mm},\ (0.9\ \text{mm})^2)$, respectively. The correlation length of the three Gaussian fields is 200 m. Then, we perform element-wise replacements in the first aperture field: elements with aperture values less than 0.6 mm are replaced with corresponding elements from the second field, and otherwise from the third field. The reservoir simulation with this specially designed fracture is considered as the synthetic reference model.

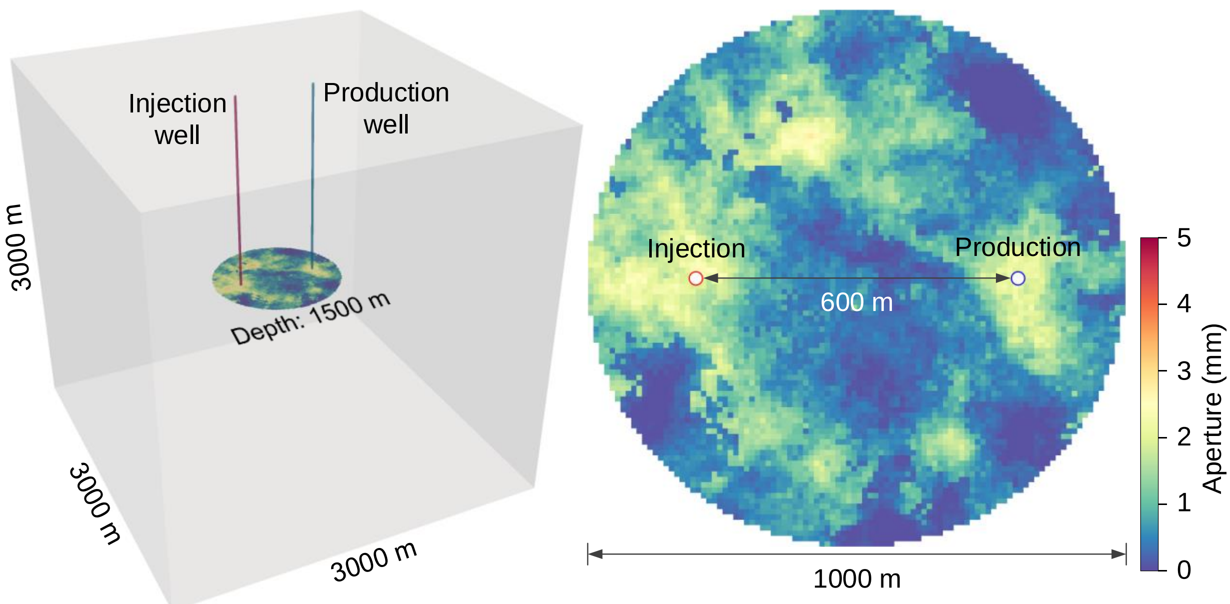

Figure 2. A synthetic field-scale EGS model with a production well and an injection well connected by a horizontal penny-shaped fracture. Left: Spatial relationship between the modeling domain, the production and injection wells, and the fracture. Right: Reference fracture aperture field.

3.2 Tracer and thermo-hydro-mechanical modeling

We utilize GEOS, a THM coupled numerical simulator developed at the Lawrence Livermore National Laboratory (Guo et al., 2016; Settgast et al., 2017, 2018), for tracer and THM modeling in this study. For tracer modeling, we first perform flow simulation to obtain fracture flow field. Subsequently, we simulate tracer transport process by solving the advection-dispersion-sorption equation based on the fracture flow field. Notice that we only consider the fracture for tracer modeling as the matrix has little impact on tracer transport owing to its relatively low permeability and the negligible matrix diffusion effect (Wu et al., 2021a). We assume an initial hydrostatic pressure in the model, setting the pressure at the fracture depth to 30 MPa. A source flux condition is imposed at the injection well with a constant flow rate of 10 L/s, and the fluid pressure at the production well is held constant at 30 MPa. Fracture boundaries are assumed impermeable.

Tracers are then released from the injection well into the fracture for one hour, followed by a 40-hour simulation of tracer transport to acquire tracer breakthrough curves at the production well. According to the suggestion from our previous study (Wu et al., 2021a), we consider both conservative and sorptive tracers to provide sufficient data for aperture inversion. For sorptive tracers, we presume an equilibrium adsorption process with a partition coefficient of 0.1 mm.

We perform THM coupled modeling to solve heat transfer process in both the fracture and the surrounding rock formations. The THM coupled model is comprised of two key solvers (Fu et al., 2016; Guo et al., 2016): the fluid and heat flow solver (TH solver), and the thermo-mechanical solver. The two solvers are managed iteratively in a one-way coupled manner. In each iteration time step, the reservoir temperature and fluid pressure fields are first obtained from the TH solver, and then the temperature field is conveyed to the thermo-mechanical solver to calculate thermal stress and update total stress of each rock matrix element. With the fluid pressure and the updated total stress, we follow Guo et al. (2016) to employ the Barton–Bandis model (Bandis et al., 1983; Barton et al., 1985) to update the thermal-drawdown induced fracture aperture w,

$$w = w_{\max} - \frac{a\sigma_n'}{1 + b\sigma_n'} \tag{2}$$

where $w_{\max}$ denotes the aperture at a zero effective stress state; σ_n' represents the effective stress normal to the fracture that equals to the difference between the total stress and the pore fluid pressure; a and b represent two material related state parameters and their detailed expressions can be found in Guo et al. (2016). Subsequently, we use the updated fracture aperture to re-invoke the TH solver for the computation of flow and temperature fields, and continue the aforementioned iterative process.

We impose zero-flux boundary conditions for fluid flow and heat transfer, as well as zero normal displacement constraints, at the model boundaries in the THM modeling. The three principal components of the in-situ stress at the fracture depth are set to 60 MPa, 90 MPa, and 54 MPa, respectively. Then, we inject relatively cool water of 50 °C with a constant flow rate of 10.0 L/s into the injection well for 50 years.

In addition, we also perform TH modeling for comparison to demonstrate the impact of thermal stress on thermal performance.

Table 1 shows the parameters for tracer and THM modeling. Since we represent the fracture plane as a thin layer in the model, the porosity and permeability of the fracture can be equivalently calculated as $\phi = w/H$ and $\kappa_f = w^3/(12H)$ respectively according to Guo et al. (2016) and Berkowitz (2002), where H is the thickness of the fracture layer. Tracer and thermal breakthrough curves for the reference model are shown in Figure 3.

Table 1 Material parameters for simulations of the field-scale EGS model

Parameter	Value
Porosity of rock matrix	0. 01
Permeability of rock matrix (m^2)	1×10^{-16}
Density of rock matrix (kg/m^3)	2,500
Rock bulk modulus (GPa)	33.3
Rock shear modulus (GPa)	20
Thermal conductivity of rock matrix (W/m/K)	2.5
Specific heat capacity of rock matrix (J/kg/K)	790
Linear thermal expansion coefficient of rock matrix (K^{-1})	8.0×10^{-6}
Density of water (kg/m^3)	887.2
Specific heat capacity of water (J/kg/K)	4,460
Compressibility of water (Pa^{-1})	5×10^{-10}
Volumetric thermal expansion coefficient of water (K^{-1})	7.66×10^{-4}
Dynamic viscosity of water (Pa·s)	1.42×10^{-4}
Diffusion coefficient (m^2/s)	1×10^{-9}
Longitudinal dispersivity (m)	0.2
Transverse dispersivity (m)	0.02
Partition coefficient (mm)	0.1

During the 40 hours of transport, the concentration distribution of the tracers exhibits distinct peaks. For conservative tracer, two peaks are observed, reflecting the heterogeneity in the reference fracture aperture field (Figure 2). This multi-peak behavior suggests the presence of multiple flow channels within the fracture. In contrast to the conservative tracer, the sorptive tracer shows delayed arrival time and smaller peak magnitude due to the sorption effect when the sorptive tracer transports along the fracture. Due to the along-path flow resistance, the simulated injection well pressure is 54.4 kPa higher than that at the production well. Both the simulated tracer breakthrough curves and the well pressure difference are used as inversion data for subsequent ES-MDA inversions to characterize fracture aperture distribution. In the present study, each tracer breakthrough curve contains 105 data points, and therefore the total inversion dataset comprises 211 data points. In our preliminary model tests, we found that the 211 observations were insufficient to properly constrain the uncertainties in fracture aperture, manifesting as the poor convergence behavior of ES-MDA. To address this issue, we empirically augment the difference between the conservative and sorptive tracer breakthrough curves into the inversion data set (Figure 3a). Such a treatment is similar to tricks used in machine learning to expand datasets, such as geometrically rotating and transforming the original data.

The comparison between TH and THM modeling indicates that thermal-drawdown induced thermal stress significantly impairs the thermal performance (Figure 3b). We adopt a threshold of 120 °C to determine the production lifespan, i.e., heat production is terminated when the production temperature decreases from the initial 200 °C to 120 °C. For the TH results, the production lifespan exceeds 50 years, while for the THM model, the production lifespan drastically reduces to 18.4 years. This substantial reduction indicates the vital role of thermal stress in EGS heat production, and neglecting it can result in significant overestimation of heat extraction potential. The two production temperature curves are used as key indicators for assessing the thermal performance prediction ability of subsequent ES-MDA inversion models.

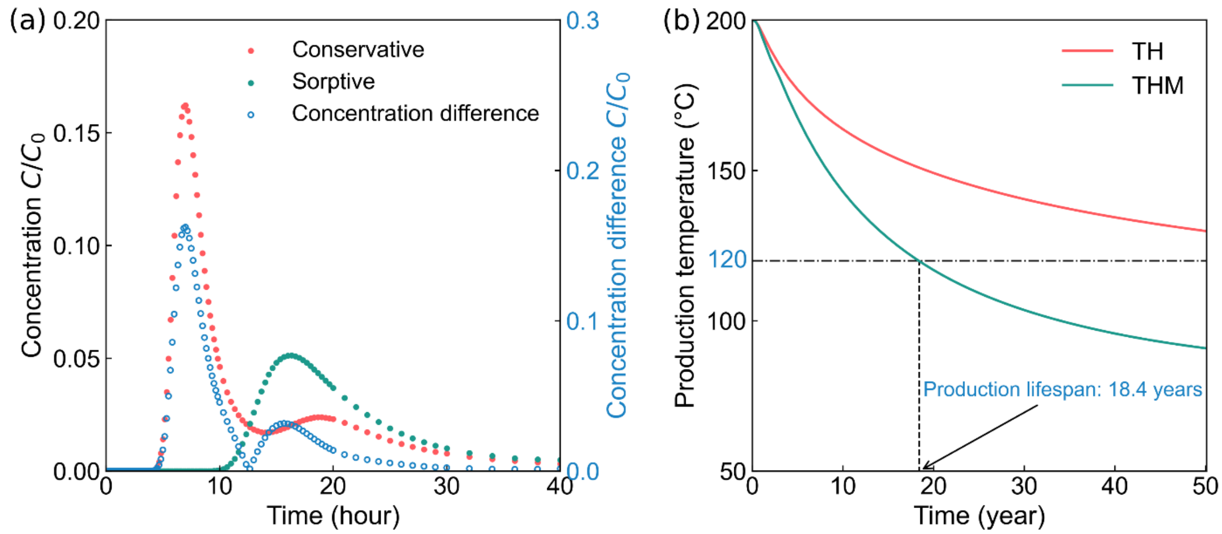

Figure 3. Tracer and thermal simulation results of the synthetic EGS model. (a) Tracer breakthrough curves measured at the production well. The measured tracer concentration is normalized by injected tracer concentration C_0. Concentration difference between the conservative and sorptive tracers is also displayed. (b) Production temperature curves obtained from the TH and THM modeling.

4 Aperture inversion and thermal prediction

We first perform a onetime aperture inversion using the previous data assimilation framework from Wu et al. (2021a), and then a multi-stage aperture inversion using the proposed inversion framework in the present study. Their results are compared in terms of aperture distribution, fracture flow field, fracture temperature distribution, as well as production temperature to demonstrate the capability of the proposed multi-stage inversion framework in dynamic aperture inversion and long-term thermal prediction.

4.1 Onetime aperture inversion and the corresponding thermal prediction

According to the data assimilation framework in Wu et al. (2021a), we first map the high dimensional aperture field to a low dimensional latent space through PCA, and then apply ES-MDA to invert for the latent parameters from the tracer and pressure data. The inferred latent parameters are then converted to an aperture field, which is then used in the 3D EGS model to solve the long-term heat extraction process.

4.1.1 Onetime aperture inversion

We use sequential gaussian simulation to generate 5,000 spatially auto-correlated aperture fields on a 1 km × 1 km domain discretized into a 100 × 100 regular grid, each following a normal distribution with a mean of 0.66 mm, a standard deviation of 0.75 mm and a correlation length of 150 m. We then apply PCA to the 5,000 aperture fields to obtain 5,000 principal components, which are arranged in descending order based on their significance, namely, percentage of preserved variance in original aperture fields. We subsequently use the first *l* principal components for aperture field generation. A larger *l* results in a more sophisticated aperture field. Based on our previous work (Wu et al., 2021a), the first 100 principal components are sufficient to preserve the primary characteristics of the original aperture field. Therefore, we set $l = 100$ for the following inversion.

We then use ES-MDA to assimilate the tracer breakthrough curves and pressure data in Figure 3a (316 data points in total). The ensemble size is set to 400, and the assimilation undergoes 12 iterations to achieve a stable inversion result. The geometric method (Emerick, 2019) is adopted to determine the inflation factor α, which is decreased by 10% after each iteration. To ensure the assimilation performance, the specification of covariances of measurement error is crucial. Here, we define measurement covariances by setting the standard deviation according to the relationship (Todaro et al., 2022): $3\sigma = p/100 \cdot y_{obs}$, where p is a user-defined parameter and y_{obs} is the observation value. We set $p = 1$, $p = 0.1$ for tracer and pressure data, respectively.

Compared with prior realizations, the posterior realizations yield tracer breakthrough curves exhibiting a significantly enhanced agreement with the reference tracer and pressure data (Figure 4). This improvement is notably evident in the alignment of peak timings, shape profiles, and overall magnitude of tracer concentration. In addition, the pressure difference between the injection and production wells simulated from the posterior realizations also matches much better with the reference values than that from the prior realizations does (Figure 4b).

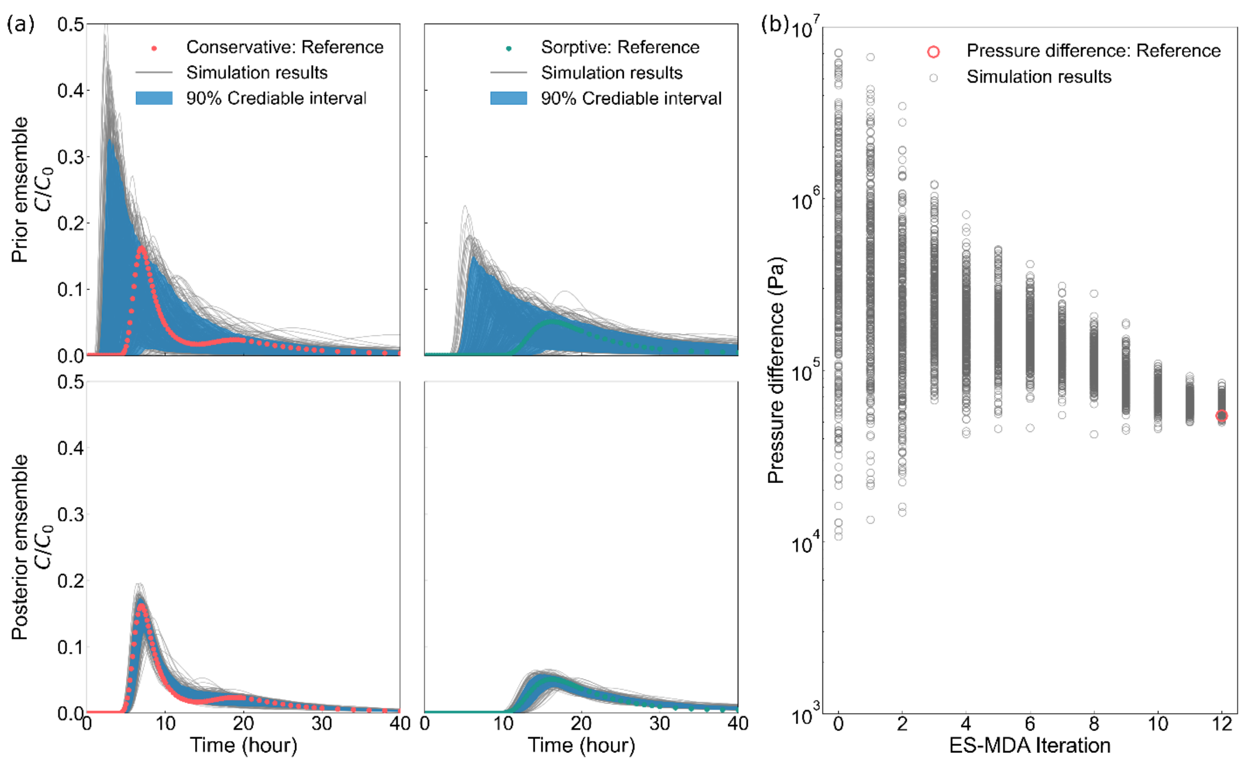

Figure 4. Numerical results of tracer and well pressure difference from prior and posterior realizations. (a) Comparison between the reference and predicted tracer breakthrough curves.

The top and bottom rows display the comparison for the prior and posterior ensembles, respectively. The simulated tracer curves are shown in gray, and the dots represent the reference tracer breakthrough data. The dark blue shadings represent the 90% credible intervals for the predicted tracer breakthrough curves. (b) Evolution of the predicted well pressure difference with ES-MDA iterations. The predicted pressure difference results are shown in gray circles, while the reference value is denoted by the red circle.

We randomly select a realization from the prior ensemble for analysis (Figure 5). The prior realization exhibits a highly dissimilar aperture distribution compared with the reference model. The following ES-MDA inversion gradually updates the aperture distribution and the obtained posterior aperture closely resembles the reference aperture (Figure 5c). The posterior model successfully resolves the primary and secondary flow channels observed in the reference flow field (as annotated in the second column in Figure 5). A major difference between the posterior and reference flow fields is the two relatively weak branch flow channels between the primary and secondary flow channels (Figure 5c). In the reference flow field, we only vaguely observe many narrow branch flow channels between the primary and secondary flow channels, while in the posterior flow field, the overall effect of these narrow branch channels seems to be represented by the two branch channels. This difference might be attributed to the insufficient characterization of detailed aperture features in the inversion aperture model.

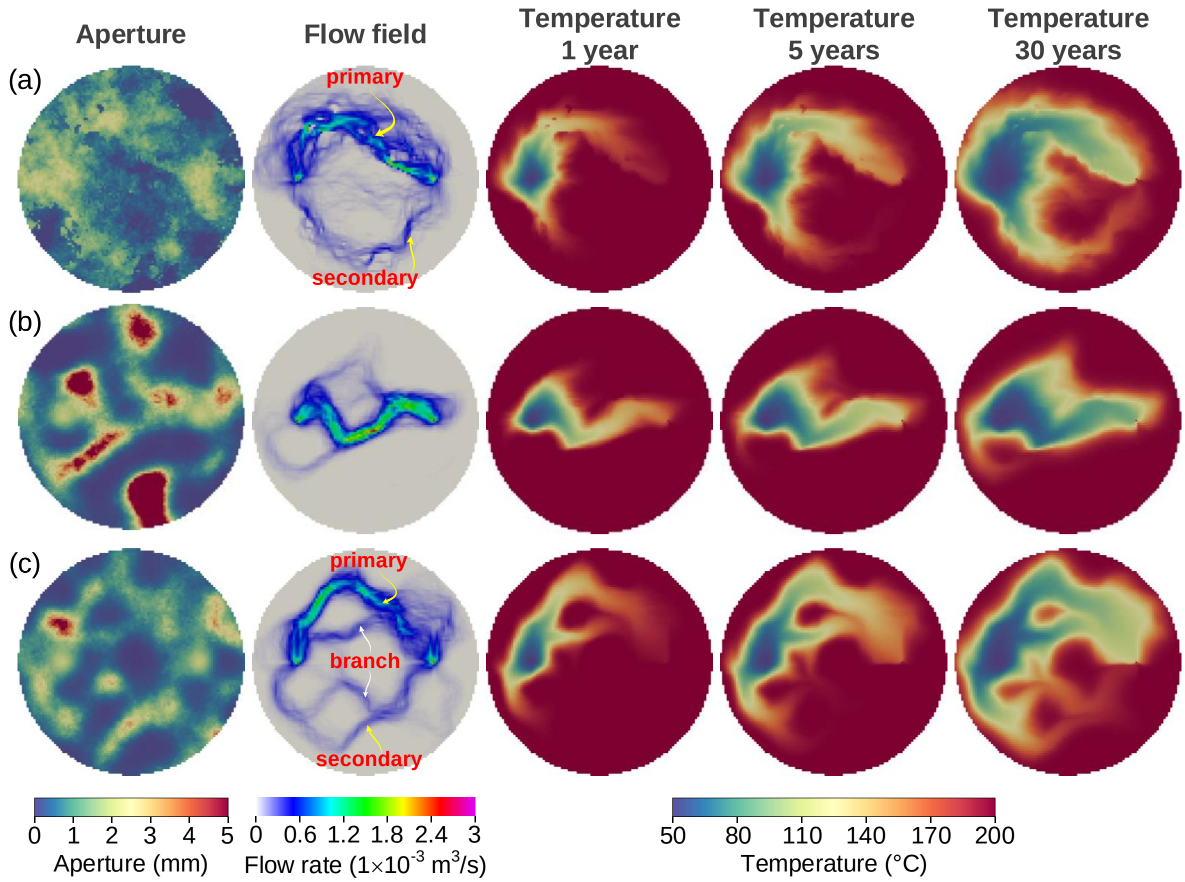

Figure 5. Comparison of aperture field, flow field, and temperature distribution within the fracture. (a) Results from the reference model. (b) Results from a randomly selected prior realization. (c) Results from the corresponding posterior realization.

4.1.2 Thermal simulation and prediction

With the prior and posterior ensembles, we then conduct thermal simulations to investigate the predictive capability of the posterior realizations in terms of EGS thermal performance. We first consider a relatively simple TH model without the mechanical process, meaning that the impact of thermal stress on aperture is ignored and the aperture field remains constant during the thermal simulation. Since the posterior realization better resolves the fracture flow pattern than the prior realization does, the fracture temperature evolution simulated with the posterior realization also resembles the reference model results better (Figure 5). The production temperature predicted by the posterior realization agrees with the production temperature of the reference model quite well (Figure 6b). Besides the selected realizations in Figure 5, we randomly select 30 additional prior realizations and their corresponding posterior realizations for TH modeling to further examine their predictive capability (Figure 6). Compared with the considerable uncertainty in thermal predictions from the prior realizations (Figure 6a), the uncertainty from the posterior realizations is significantly reduced, and most of the posterior production temperature curves reasonably match the reference temperature curve.

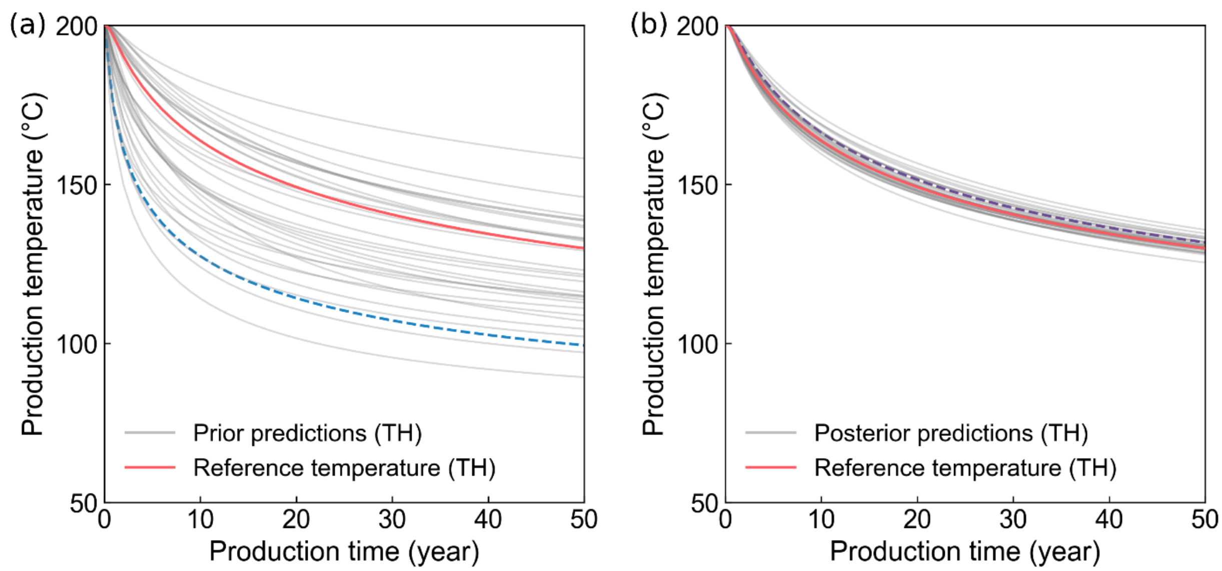

Figure 6. Predictions of production temperature from TH simulation for the randomly selected 30 prior (a) and posterior (b) realizations. The gray solid lines represent the results for the randomly selected realizations from the prior and posterior ensembles. The red solid line indicates the production temperature for the reference model from TH simulation. The blue dashed line in (a) is the production temperature curve for the selected prior realization in Figure 5, and its corresponding posterior curve is denoted by the dashed purple line in (b).

4.1.3 Effects of thermal stress on aperture evolution and thermal performance

The above results indicate that the posterior realizations can properly predict long-term thermal performance under the constant aperture scenario (i.e., TH model). However, in a more realistic scenario that incorporates mechanical process, fracture aperture will dynamically evolve under the thermoporoelastic effect (Gee et al., 2021; Guo et al., 2016). To further verify the predictive capability of the posterior realizations under the impact of thermoporoelastic effect, we perform THM simulations using the randomly selected realizations in Figure 5. We compare the aperture distribution, fracture flow field as well as fracture temperature distribution at different production times between the posterior and reference models (Figure 7). Due to the presence of thermal stress, the aperture fields in both the posterior and reference models evolve significantly during heat extraction, and the fracture flow fields gradually become more and more concentrated, i.e., thermal-drawdown induced flow channeling (Guo et al., 2016). Since heat transfer highly relies on fracture flow pattern, flow channeling reduces effective heat transfer area and accelerates thermal breakthrough (Figure 7). Compared with the results from TH modeling, the production temperature from THM modeling decreases remarkably, for both the reference model and the posterior realizations (Figure 8).

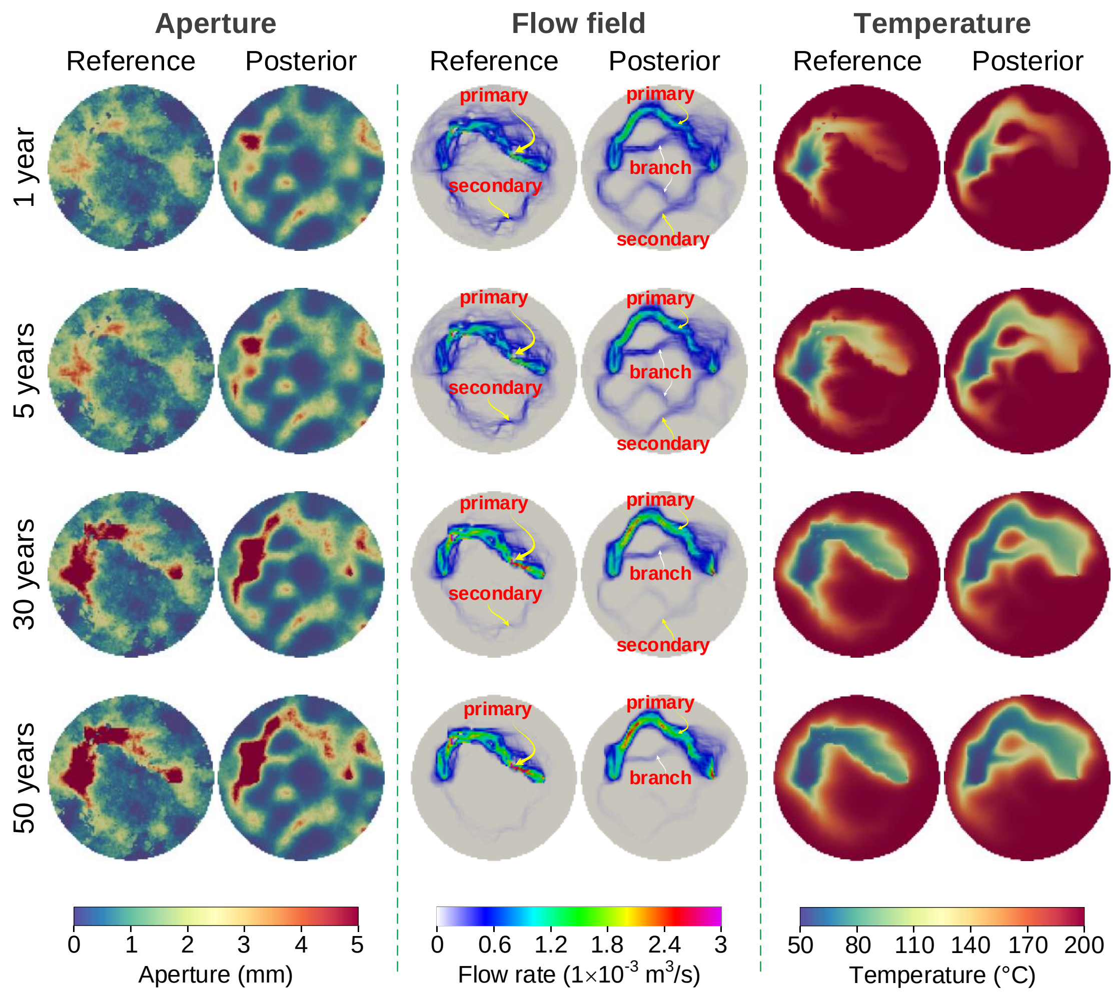

Figure 7. Evolution of fracture aperture, flow field, and fracture temperature in THM simulations. Both the reference model and the selected posterior realization from Figure 5 are shown.

An interesting observation is that the evolution of aperture and flow fields from the posterior realization is similar to that from the reference model (Figure 7). After 30 years production, both the reference and posterior models show a dominating flow channel between the injection and production wells. The secondary channel almost disappears in both posterior and reference realizations. However, there exists a major difference of the flow field between the reference and posterior models, that a branch flow path still exists alongside the dominating channel from the posterior realization but not in that from the reference model. The effect of this branch flow path on thermal performance is nonnegligible as it increases the effective heat transfer area between fluid and rock formation (temperature distribution in Figure 7). With the consideration of dynamic aperture evolution, the predicted production temperature from the posterior realization gradually deviates from the reference result (Figure 8b). Specifically, due to the presence of the branch flow channel, the posterior realizations tend to exhibit a relatively slower thermal breakthrough compared with the reference model. Such a result indicates that although the posterior realization is able to capture the primary features of the initial flow field in the reference model by fitting tracer data, it may produce a biased flow field due to the dynamic variation of the aperture field during heat extraction, ultimately leading to an overestimated production temperature.

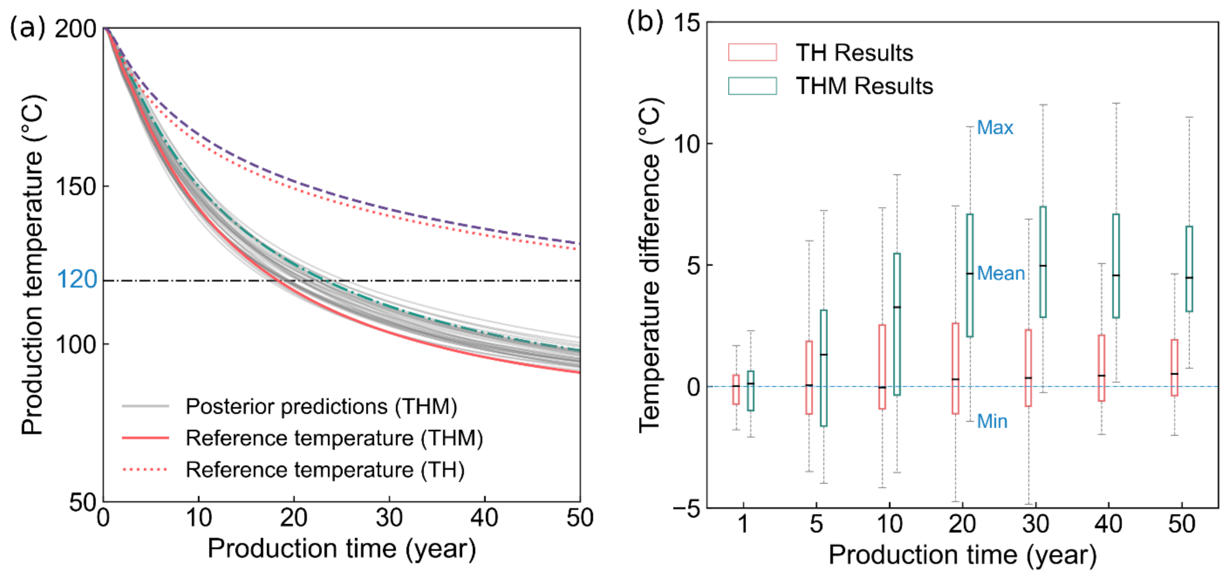

Figure 8. Predictions of production temperature from THM simulation for the randomly selected 30 posterior realizations. (a) Temperature breakthrough cuves from the reference model and posterior realizations. The green dashdot line is the production temperature curve obtained from the selected posterior realization shown in Figure 7, and its corresponding curve from TH simulation is represented by the purple dashed line for comparison. (b) Difference in heat production temperature between the reference and the 30 posterior realizations at different production times. TH and THM results are compared. The box plots show the maximum, minimum and mean of temperature difference.

4.2 Multi-stage aperture inversion and the corresponding thermal prediction

The above analysis demonstrates that ignoring the dynamic evolution of fracture aperture during inversion renders the posterior model with compromised long-term thermal prediction capability. To assess the capability of the proposed multi-stage inversion framework in capturing dynamic aperture evolution, we further performed the second and third tracer inversions after five and fifteen years production.

4.2.1 Second aperture inversion

We first use the aperture field from the reference model after five years production (Second row, first column in Figure 7) to generate a new tracer and pressure dataset for the second aperture inversion. Model parameters and tracer injection conditions are the same as that used for the first tracer modeling at the initial stage (Table 1). Due to the variation of fracture aperture and flow field, both the conservative and sorptive tracer breakthrough curves exhibit noticeable changes in terms of peak magnitude and the arrival time of the peak (Figure 9). For the conservative tracer, the arrival time is slightly delayed, accompanied by a reduction in its peak magnitude. The secondary peak becomes almost negligible as most of the injected fluid concentrates in the primary flow channel corresponding to the first peak. Conversely, for the sorptive tracer, the arrival time slightly advances, along with an increase in peak magnitude. The pressure difference between the injection and production wells decreases significantly from 54.4 kPa to 24.24 kPa because of the increase of fracture aperture under the thermal stress effect.

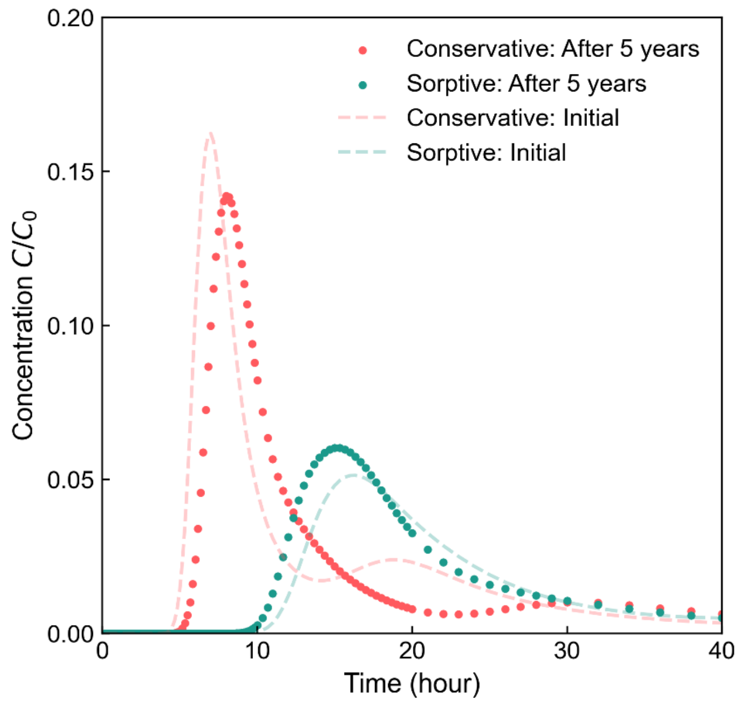

Figure 9. Tracer breakthrough curves obtained from the reference model. The dashed lines are the tracer results from the initial aperture field while the dots represent the tracer results after 5 years production.

The second inversion follows the same steps as the initial inversion. Note that tracer dataset is still augmented by adding the difference between the conservative and sorptive tracer breakthrough curves to achieve an appropriate inversion result. The settings for measurement errors remain consistent with those of the initial inversion. Through the initial ES-MDA inversion, we have acquired a posterior ensemble that successfully resolves the initial fracture flow pattern, and therefore it is appropriate to use the posterior ensemble as the prior ensemble for this second inversion. It is noteworthy that at the fifth year of heat production, the impact of thermal stress is not particularly pronounced such that the changes in the fracture aperture field are limited compared to the initial state and the majority of features remain preserved (Figure 7).

Therefore, the secondly inversed fracture apertures should, theoretically, not deviate excessively from the one in the first inversion. In this regard, we suggest adopting the following modification scheme to update the latent parameters during the ES-MDA inversion process,

$$\mathbf{z}_j^i = \mathbf{z}_j^{i-1} + \gamma \mathbf{C}_{\mathrm{ZY}}^{i-1} (\gamma \mathbf{C}_{\mathrm{YY}}^{i-1} + \alpha_i \mathbf{R})^{-1} (\mathbf{y}_{\mathrm{obs}} + \sqrt{\alpha_i} \boldsymbol{e}_j - \mathbf{y}_j^{i-1}) \quad (3)$$

where γ is a user-defined parameter to scale the error variance $\mathbf{C}_{\mathrm{ZZ}}$ of latent parameter $\mathbf{z}$, which is set to 0.02 in this study. The modified formula is inspired by the ensemble representation of model gradient in the derivation of the ES-MDA algorithm (Evensen, 2018).

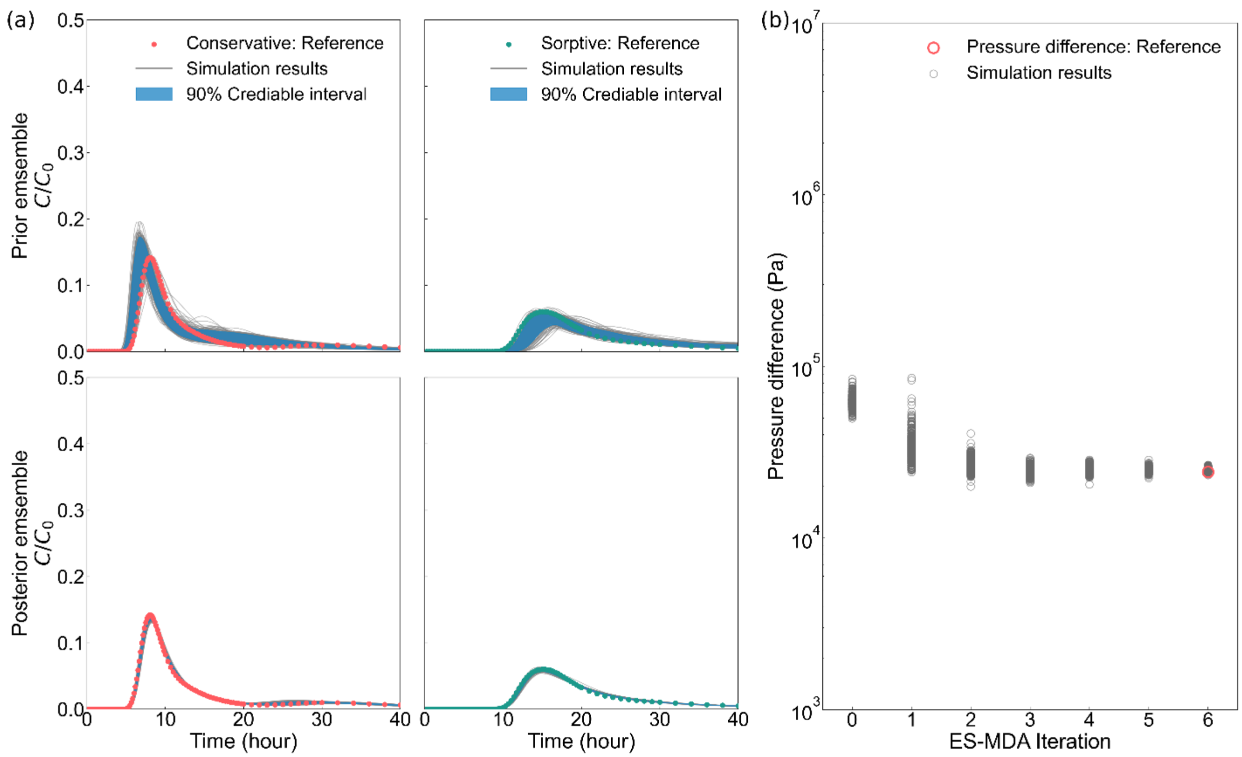

Figure 10. Numerical results of tracer and well pressure difference from the prior and posterior realizations for the second inversion. (a) Comparison between the reference and predicted tracer breakthrough curves. (b) Evolution of the predicted well pressure difference with ES-MDA iterations.

Since the initial aperture/flow fields share many common features with the aperture/flow fields after five years production (Figure 7), the uncertainty of the prior results is relatively low (Figure 10). The inversion achieves a stable result after six iterations. Posterior realizations from the second inversion match perfectly with the reference model in terms of tracer breakthrough and well pressure difference (Figure 10). We still use the selected realization in Figure 5 to analyze the aperture and flow fields. The posterior aperture/flow fields from the second inversion closely resemble that from the initial inversion, but with appropriate local modifications to match the tracer and pressure data obtained at the fifth year of production (Figure 11). An important modification in the flow field is that the primary flow channel undergoes slight downward movement, and one of the branch flow paths almost disappears, making the overall flow field more similar to the reference flow field compared with that from the initial inversion.

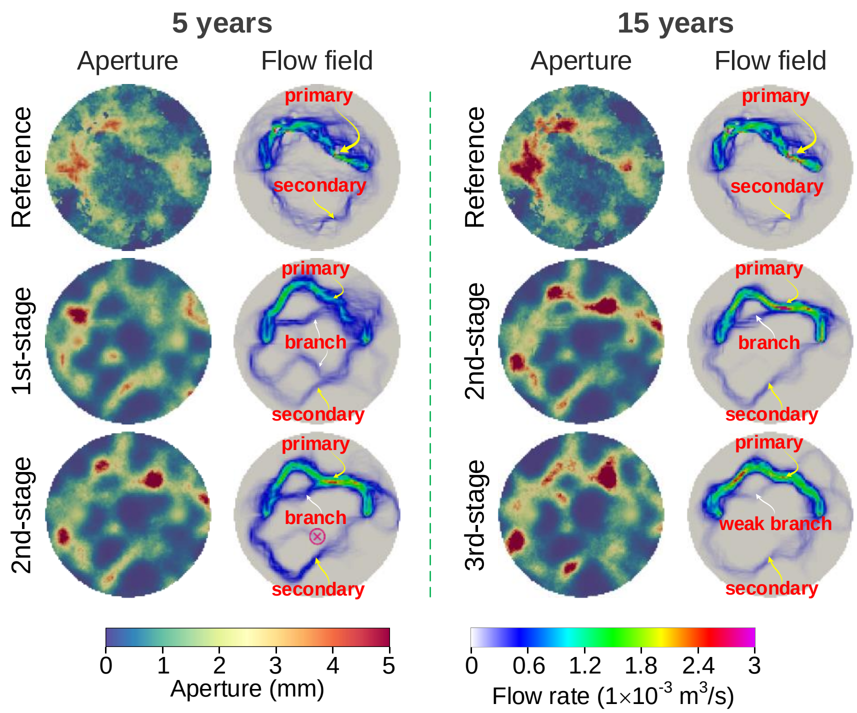

Figure 11. Comparison of the fracture aperture and flow field at the fifth and fifteenth year of production between the reference model and the selected posterior realization. At the fifth year, we compare the results from the first stage (initial stage) and the second stage to illustrate the change of aperture and flow fields due to the second inversion. At the fifteenth year, we compare the results from the second and third stages to illustrate the change caused by the third inversion.

4.2.2 Thermal prediction with the posterior ensemble from the second inversion

We then use the posterior realizations from the second inversion to perform a second-stage THM simulation to model the thermal process of the EGS model after the fifth year. Note that the temperature field at the fifth year simulated by the posterior realizations from the first inversion is used as the initial temperature field for this second-stage THM simulation. We compare the reference model with the selected posterior realization (from the second inversion) in terms of aperture field, flow field and fracture temperature distribution at the 5th, 15th, 30th and 50th year respectively (Figure 12). As one of the branch flow channel resolved by the initial inversion merges into the secondary flow channel, the effective heat transfer area is reduced and the fracture temperature distributions (eighth column in Figure 12) modeled by the posterior realization after the second inversion resemble the reference model results better than that modeled by the posterior realization after the first inversion (sixth column in Figure 7). The predicted production temperature from the second inversion stage is lower than the previous predictions from the first inversion stage, and agrees better with the reference temperature breakthrough curve (Figure 13).

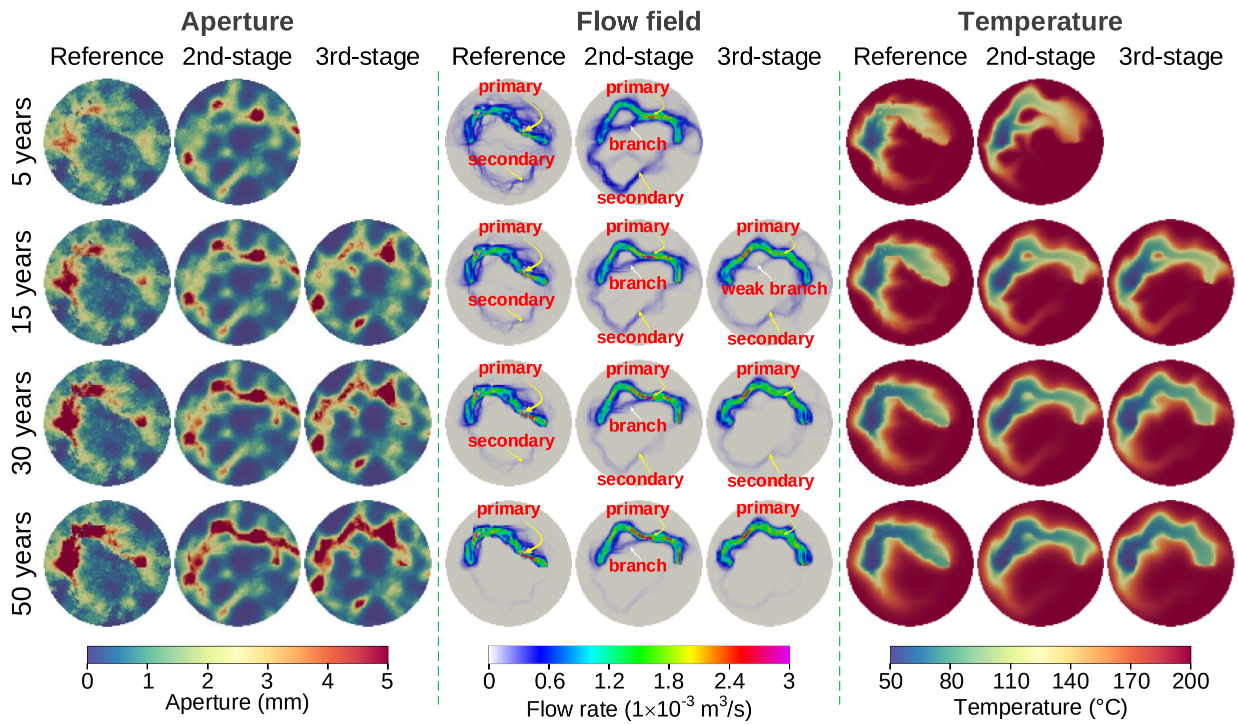

Figure 12. Comparison of fracture aperture, flow field, and temperature distribution between the reference model and the selected posterior realization after the second and third inversions.

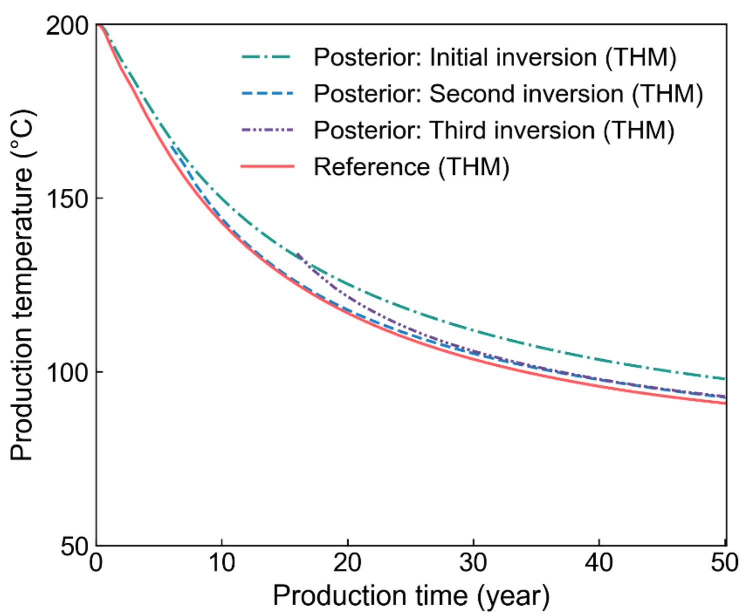

Figure 13. Production temperature for the reference model, as well as the selected posterior realizations after the initial, second and third inversions. Note that the temperature curves for the posterior realizations after the second and third inversions start from the fifth and fifteenth year, respectively.

We further examine thermal predictions from the previously selected 30 realizations after the second inversion (Figure 14). The prediction uncertainty decreases remarkably compared with the predictions after the initial inversion. Although there is a sudden and subtle change in the predicted temperature curve at the fifth year (Figure 14a) due to the sudden change of fracture aperture, the overall long-term thermal performance under the thermal-hydro-mechanical coupled conditions is appropriately covered by the posterior predictions from the 30 realizations. We also calculate the production lifespan of the EGS model according to the predicted temperature curves (Figure 14b). As annotated in Figure 14b, the production lifespan of the reference model is 18.4 years, and the average production lifespan predicted by the posterior predictions after the second inversion (20.0 years) is more accurate than that predicted by the posterior predictions after the initial inversion (21.3 years). More importantly, the prediction range of the production lifespan reduces from 17.4-25.5 years for the first inversion, to 18.6-21.9 years for the second inversion.

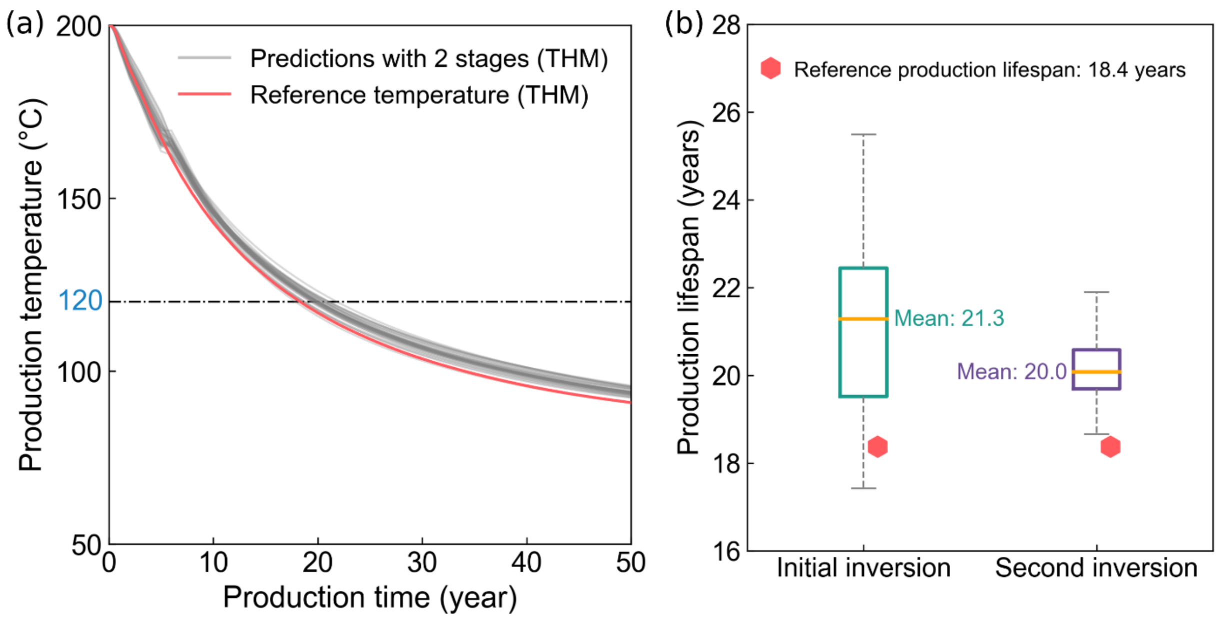

Figure 14. Predictions of production temperature from THM simulation for the randomly selected 30 posterior realizations after the second inversion. (a) Temperature breakthrough cuves from the reference model and posterior realizations. Note that predictions at the first five years are obtained from the initial inversion, while predictions after the fifth year are from the second inversion. (b) Comparison of heat production lifespan between the reference and posterior realizations. Both the results from the initial and second inversions are shown.

4.2.3 Third aperture inversion

As the second inversion shows a remarkable improvement in thermal prediction, we further perform a third inversion at the fifteenth year of production (Figure 12). The posterior ensemble from the second inversion is employed as the prior ensemble for the third inversion. Given the favorable match of the flow field obtained in the second inversion with the reference model, the third inversion theoretically requires only minor adjustments on the aperture fields from the second inversion. Therefore, we continue to adopt the scaling approach, as discussed in

Section 4.2.1, for the error variance ($\mathbf{C}_{zz}$) of latent parameters, with the scale parameter γ set as 0.004. The third inversion quickly yields a stable result after six iterations (Figure 15). A key modification is that the branch channel alongside the primary channel is further weakened, making the overall flow field even closer to the reference flow field compared with that from the second inversion (Figure 11).

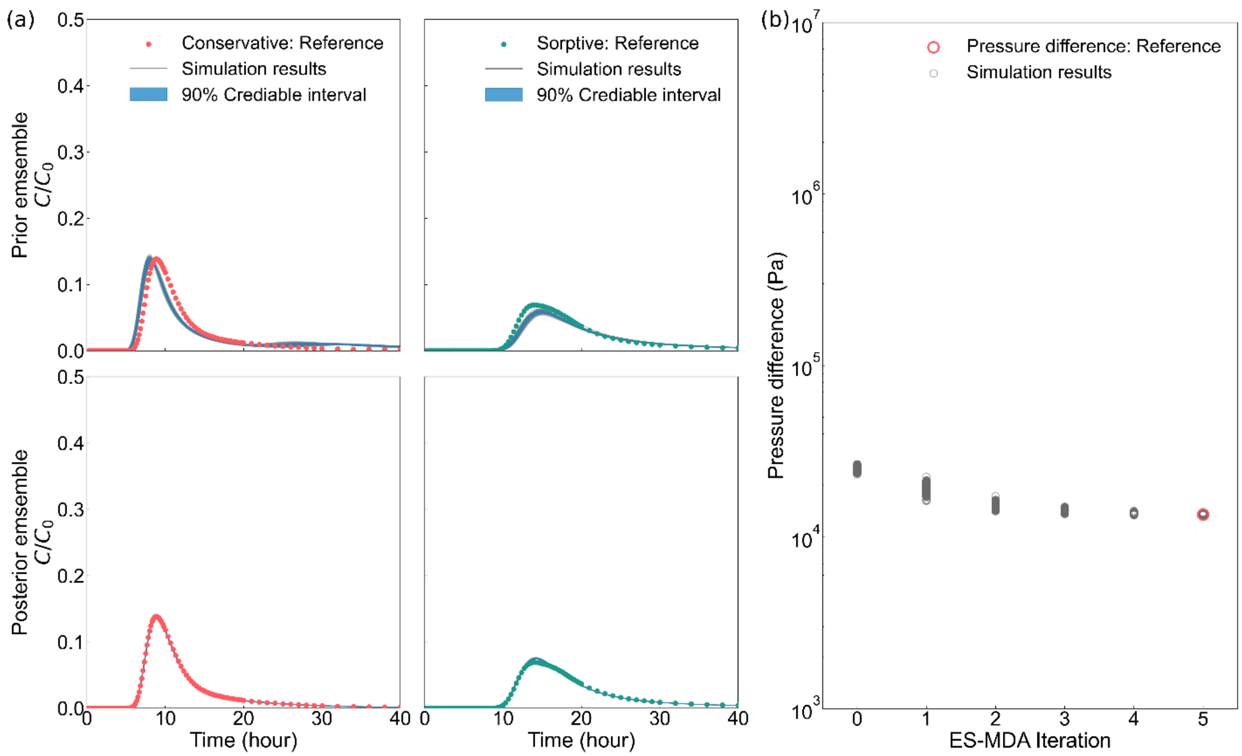

Figure 15. Numerical results of tracer and well pressure difference from the prior and posterior realizations for the third inversion.

4.2.4 Thermal prediction with the posterior ensemble from the third inversion

We then perform THM simulations using the posterior realizations from the third inversion to predict the thermal performance of the EGS model after 15 years. The temperature field at the fifteenth year simulated by the second-stage realizations is used as the initial temperature field for this third-stage THM simulation. We compare the selected posterior realizations from the second and third inversions with the reference model in terms of aperture/flow fields and fracture temperature distribution at the 15th, 30th and 50th year respectively (Figure 12). As a result of localized modification in the aperture field during the third inversion, the branch flow path that appears in the second inversion progressively diminishes and merges into the primary channel. Such a modification further enhances the thermal prediction capability of the inversion model, mainly manifesting as the reduction of prediction uncertainty Figure 16. Notice that there are discontinuities in the predicted temperature curve at the fifteenth year between the second and third inversion realizations due to the sudden modification of fracture aperture (Figure 13 and 16). However, this discontinuity swiftly stabilized. After 20 years, the thermal production curve closely resembles the reference curve, with an overall average temperature error less than 3 °C (Figure 16b). This is mainly attributed to the correction to the branch flow channel in the third inversion, leading to a further reduction in the effective heat transfer area.

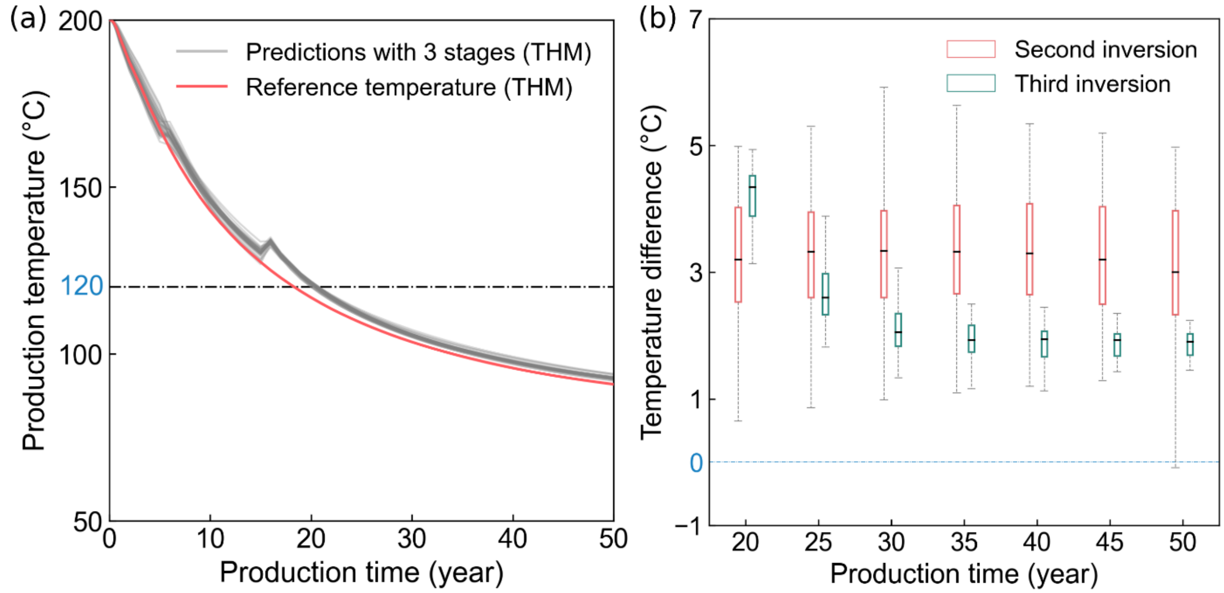

Figure 16. Predictions of production temperature from THM simulation for the randomly selected 30 posterior realizations after the third inversion. (a) Temperature breakthrough curves from the reference model and posterior realizations. Note that predictions at the first five years are obtained from the initial inversion, while predictions between years five and fifteen are obtained from the second inversion, and predictions after the fifteenth year are from the third inversion. (b) Comparison of the production temperature difference between the reference and posterior realizations. Both the results from the second and third inversions are shown.

5 Discussions

5.1 When to perform the second and subsequent aperture inversions?

The proposed multi-stage inversion framework requires to perform multiple inversions during the operation of an EGS to accommodate the continuously varying reservoir conditions, i.e., dynamic fracture aperture evolution in the current study. Except for the initial inversion which is generally performed before heat extraction, the timing of subsequent inversions is an essential decision that needs to be carefully determined. For the EGS model in this study, we perform the second and third inversion at the fifth and fifteenth years after the commencement of heat extraction respectively. The two timings appear to be appropriate as the long-term thermal performance is accurately predicted after the second and third aperture inversions (Figure 16).

In real-world applications, as a tracer testing can be completed in several weeks or months and the cost of tracer testing is relatively low compared with that of drilling and long-term thermal operations, we could conduct tracer testing every year and perform frequent aperture inversion accordingly on a yearly base. Nevertheless, the necessity of such a frequent tracer testing and aperture inversion should be carefully considered. Since thermal conduction in rock formations is relatively slow, it generally requires a considerable amount of time to develop significant thermal stress to alter fracture aperture field and affect thermal performance remarkably. This is evident from the thermal performance comparison in Figure 8a that the thermal curves predicted by the posterior realizations are very close to the reference thermal curves within the first several years. Therefore, although economically and technically viable, it is unnecessary to repeat tracer testing and aperture inversion too frequently. However, the time interval between two consecutive inversions should not be too long either, otherwise the thermal prediction during this time interval might significantly deviates from field measurements. To examine the effect of inversion timing on thermal prediction, we perform a second-stage inversion at the tenth year (Figure 17). The predicted production temperature at the tenth year shows considerable uncertainty compared with that in Figure 14 where the second-stage inversion happens at the fifth year. In addition, as the simulated temperature field at the end of the first inversion stage is used as the initial temperature field for THM modeling in the second stage, a large inversion time interval may lead to a significant deviation in temperature field, which may further compromise the thermal prediction capability of the inversion results. The second-stage inversion at the tenth year ultimately results in an underestimated thermal performance (Figure 17).

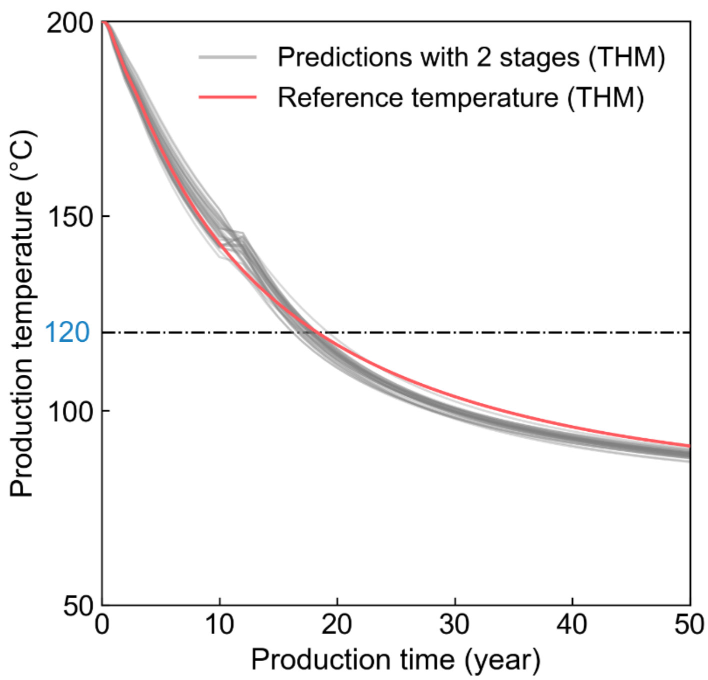

Figure 17. Temperature breakthrough curves from the reference model and the randomly selected 30 posterior realizations after a second stage inversion at the tenth year.

The timing of the second tracer testing and aperture inversion highly depends on the hydrogeological conditions of EGS reservoirs. For the single-fracture EGS model in the current study, a second-stage tracer testing and aperture inversion at the fifth year appears to be a reasonable choice, and two or three inversion stages seem to be sufficient to provide accurate long-term thermal predictions. In real-world applications, a straightforward principle to determine the inversion timing is to compare the simulated production temperature with field measurements. In presence of a large temperature difference, a new tracer testing can be performed to provide new data for another round of inversion to correct fracture aperture field.

5.2 Chemical reactions induced aperture evolution

The present study focuses on the impact of thermal stress on fracture aperture evolution. As pointed out in the literature, there are some other processes, such as chemical reactions, that may also induce significant aperture alterations during heat extraction from EGSs (Ameli et al., 2014; Pandey et al., 2014; Xu et al., 2004). The injection of low-temperature fluids into EGS reservoirs alters the chemical balance of pre-existing minerals, leading to mineral dissolution and precipitation on fracture surfaces. Coupled simulations investigating chemical reaction effects reveal that dissolution may enlarge fracture aperture, while precipitation tends to reduce aperture (Pandey et al., 2018; Salimzadeh & Nick, 2019; Song et al., 2022). The behavior and extent of chemical reactions in fractured reservoirs depend strongly on the host rock composition, fractural flow, and temperature fields.

Our proposed multi-stage inversion framework is capable of addressing chemical reactions-induced aperture change during fracture inversion. In practical applications, inversions can be conducted at different production times to capture evolutions in fracture aperture resulting from chemical reactions. Between two inversion stages, the THM solver can be approximately employed for thermal prediction, eliminating the need to directly simulate the impact of chemical reactions on thermal performance. This approximation is reasonable because in most existing geothermal power plants located in sandstone and granite reservoirs, the chemical reactions occur much more slowly in comparison to thermoporoelastic effects, typically over a longer time scale (Pandey et al., 2014; Rawal & Ghassemi, 2014). However, in carbonate geothermal reservoirs, chemical reactions may proceed at a relatively fast pace (Goldscheider et al., 2010; Pandey et al., 2014). Relying solely on updating fracture apertures at each inversion stage and without explicitly simulating the effects of chemical reactions in the actual thermal simulation may lead to a reduction in the accuracy of heat production predictions within each stage. For such scenarios, we need to enrich the forward model to include chemical reactions module and necessary couplings with other physical fields, and thus the proposed inversion framework could still be applied for dynamic aperture inversion and thermal prediction.

5.3 Implications for dynamic reservoir characterization

The dynamic evolution of rock properties due to complex thermo-hydro-mechanical-chemical coupled processes is well acknowledged in a broad range of subsurface reservoir applications, such as oil and gas extraction, CO_2 geological sequestration, waste water disposal, nuclear waste disposal, as well as geothermal energy recovery presented in this study. An accurate characterization of the dynamic evolution of key reservoir parameters, including permeability, porosity, and fracture aperture, is essential for the modeling and prediction of reservoir performance. However, due to the inherent geological and physical/chemical complexities associated with subsurface reservoirs, the characterization of reservoir parameters is quite challenging, and most previous studies actually ignored the dynamic evolution of these parameters. The current study provides a novel method to infer the dynamic evolution of reservoir parameters through a newly proposed multi-stage inversion framework. The feasibility of the framework is tested through a synthetic EGS model, in which the dynamic evolution of fracture aperture caused by THM coupled processes is appropriately captured through the inversion of tracer data. Given the flexibility of the proposed framework, it can be easily extended to the dynamic characterization of other reservoir parameters, such as rock permeability, porosity, and oil saturation, as long as a forward model connecting these parameters with available field measurements can be developed.

Our current work primarily focuses on employing tracer data for reservoir inversion. Tracer tests, owing to their low cost and convenience of execution, are suitable for multiple tests in practical applications, making the proposed multi-stage inversion using tracer data applicable for real-world reservoir development. In addition to tracer data, other geophysical data, including seismic and electrical data, can also be repeatedly obtained with relatively low cost once the relevant sensors and devices are installed in the field. Therefore, these geophysical data are also suitable for the proposed multi-stage inversion framework, and can be used either separately or jointly with tracer data to provide further constraints on reservoir parameters. More importantly, as seismic and electrical data depend not only on flow properties but also on rock mechanical properties, the incorporation of seismic and electrical data may enable the dynamic characterization of other reservoir parameters such as rock modulus and water/oil saturation. Of course, the extension of the proposed framework to the characterization of other reservoir parameters using various geological, geophysical and hydrogeological data requires further investigation and verification.

6 Conclusions

This study proposes a multi-stage data assimilation framework to capture the dynamic evolution of fracture aperture during heat extraction from EGS reservoirs, and thus provide accurate long-term thermal predictions to guide field operations and optimizations. The framework involves multiple aperture inversions performed at different times throughout the lifetime of EGS reservoirs. In each inversion, we use ES-MDA method to invert for fracture aperture distribution from tracer and pressure data. Between two consecutive inversion stages, the later inversion stage utilizes the posterior aperture ensemble from the previous stage as the prior ensemble, enabling a progressively refined characterization of the fracture apertures. The temperature field obtained at the end of the previous THM simulation serves as the initial temperature field for the subsequent THM simulation, ensuring continuous long-term thermal performance predictions.

A synthetic field-scale single-fracture EGS model is developed to demonstrate the efficacy of the proposed framework. Compared with previous one-time inversion, the proposed multi-stage inversion strategy effectively captures the dynamic evolution of fracture apertures and flow patterns. As a result, the accuracy of long-term heat performance predictions is enhanced, and the associated uncertainties are significantly reduced. Numerical results also show the importance of selecting an appropriate inversion timing. For the single-fracture EGS model in this work, two to three inversion stages seem to be sufficient, and performing the second and third stages at the fifth and fifteenth years appears to be appropriate.

Since this study mainly focuses on single dominant fracture inversions and only considers the case of one injection well and one production well, it would be meaningful to extend the current framework to accommodate complex fracture networks and multi-well EGS reservoir applications. Additionally, we use conservative and sorptive tracer data for inversion. Although proved to be useful, the two types of data do not contain any temperature information, and it would be worth exploring in the future the use of thermo-sensitive tracers to further improve fracture characterization and thermal prediction in EGSs.

Acknowledgments

The authors would like to greatly acknowledge the National Natural Science Foundation of China (Project No. 42372305), the National Key Research and Development Program of China (No. 2021YFA0716000) and the China National Petroleum Corporation-Peking University Strategic Cooperation Project of Fundamental Research.

Data Availability Statement

The multiphysics simulator GEOS used in this study for tracer, thermo-hydro-mechanical modeling is open sourced and is available at https://github.com/GEOS-DEV/GEOS (Settgast et al., 2018). The computer codes and data used for fracture aperture inversion are available at https://doi.org/10.5281/zenodo.10417269 (Zhang & Wu, 2023).

References

Abbaszadeh-Dehghani, M., & Brigham, W. E. (1984). Analysis Of Well-to-Well Tracer Flow To Determine Reservoir Layering. *Journal of Petroleum Technology*, *36*(10), 1753–1762. https://doi.org/10.2118/10760-PA

Ameli, P., Elkhoury, J. E., Morris, J. P., & Detwiler, R. L. (2014). Fracture Permeability Alteration due to Chemical and Mechanical Processes: A Coupled High-Resolution Model. *Rock Mechanics and Rock Engineering*, *47*(5), 1563–1573. https://doi.org/10.1007/s00603-014-0575-z

Bandis, S. C., Lumsden, A. C., & Barton, N. R. (1983). Fundamentals of rock joint deformation. *International Journal of Rock Mechanics and Mining Sciences & Geomechanics Abstracts*, *20*(6), 249–268. https://doi.org/10.1016/0148-9062(83)90595-8

Barton, N., Bandis, S., & Bakhtar, K. (1985). Strength, deformation and conductivity coupling of rock joints. *International Journal of Rock Mechanics and Mining Sciences & Geomechanics Abstracts*, *22*(3), 121–140. https://doi.org/10.1016/0148-9062(85)93227-9

Berkowitz, B. (2002). Characterizing flow and transport in fractured geological media: A review. *Advances in Water Resources*, *25*(8), 861–884. https://doi.org/10.1016/S0309-1708(02)00042-8

Chandna, A., & Srinivasan, S. (2022). Mapping natural fracture networks using geomechanical inferences from machine learning approaches. *Computational Geosciences*, *26*(3), 651–676. https://doi.org/10.1007/s10596-022-10139-5

Chen, J., Xu, T., Liang, X., & Jiang, Z. (2022). Stochastic inversion of tracer test data with seismicity constraint for permeability imaging in enhanced geothermal reservoirs. *Geophysics*, *87*(6), M307–M319. https://doi.org/10.1190/geo2022-0130.1

Detwiler, R. L. (2008). Experimental observations of deformation caused by mineral dissolution in variable-aperture fractures. *Journal of Geophysical Research: Solid Earth*, *113*(B8). https://doi.org/10.1029/2008JB005697

Egert, R., Korzani, M. G., Held, S., & Kohl, T. (2020). Implications on large-scale flow of the fractured EGS reservoir Soultz inferred from hydraulic data and tracer experiments. *Geothermics*, *84*, 101749. https://doi.org/10.1016/j.geothermics.2019.101749

Elahi, S. H., & Jafarpour, B. (2018). Dynamic Fracture Characterization From Tracer-Test and Flow-Rate Data With Ensemble Kalman Filter. *SPE Journal*, *23*(02), 449–466. https://doi.org/10.2118/189449-PA

Emerick, A. A. (2019). Analysis of geometric selection of the data-error covariance inflation for ES-MDA. *Journal of Petroleum Science and Engineering*, *182*, 106168. https://doi.org/10.1016/j.petrol.2019.06.032

Emerick, A. A., & Reynolds, A. C. (2013). Ensemble smoother with multiple data assimilation. *Computers & Geosciences*, *55*, 3–15. https://doi.org/10.1016/j.cageo.2012.03.011

Evensen, G. (2018). Analysis of iterative ensemble smoothers for solving inverse problems. *Computational Geosciences*, *22*(3), 885–908. https://doi.org/10.1007/s10596-018-9731-y

Fu, P., Hao, Y., Walsh, S. D. C., & Carrigan, C. R. (2016). Thermal Drawdown-Induced Flow Channeling in Fractured Geothermal Reservoirs. *Rock Mechanics and Rock Engineering*, *49*(3), 1001–1024. https://doi.org/10.1007/s00603-015-0776-0

Gee, B., Gracie, R., & Dusseault, M. B. (2021). Multiscale short-circuiting mechanisms in multiple fracture enhanced geothermal systems. *Geothermics*, *94*, 102094. https://doi.org/10.1016/j.geothermics.2021.102094

Ghassemi, A., & Suresh Kumar, G. (2007). Changes in fracture aperture and fluid pressure due to thermal stress and silica dissolution/precipitation induced by heat extraction from subsurface rocks. *Geothermics*, *36*(2), 115–140. https://doi.org/10.1016/j.geothermics.2006.10.001

Goldscheider, N., Mádl-Szőnyi, J., Erőss, A., & Schill, E. (2010). Review: Thermal water resources in carbonate rock aquifers. *Hydrogeology Journal*, *18*(6), 1303–1318. https://doi.org/10.1007/s10040-010-0611-3

Guo, B., Fu, P., Hao, Y., Peters, C. A., & Carrigan, C. R. (2016). Thermal drawdown-induced flow channeling in a single fracture in EGS. *Geothermics*, *61*, 46–62. https://doi.org/10.1016/j.geothermics.2016.01.004

Jiang, Z., Ringel, L. M., Bayer, P., & Xu, T. (2023). Fracture Network Characterization in Reservoirs by Joint Inversion of Microseismicity and Thermal Breakthrough Data: Method Development and Verification. *Water Resources Research*, *59*(9), e2022WR034339. https://doi.org/10.1029/2022WR034339

Jiang, Z., Zhang, S., Turnadge, C., & Xu, T. (2021). Combining autoencoder neural network and Bayesian inversion to estimate heterogeneous permeability distributions in enhanced geothermal reservoir: Model development and verification. *Geothermics*, *97*, 102262. https://doi.org/10.1016/j.geothermics.2021.102262

Le, D. H., Emerick, A. A., & Reynolds, A. C. (2016). An Adaptive Ensemble Smoother With Multiple Data Assimilation for Assisted History Matching. *SPE Journal*, *21*(06), 2195–2207. https://doi.org/10.2118/173214-PA

Li, S., Wang, S., & Tang, H. (2022). Stimulation mechanism and design of enhanced geothermal systems: A comprehensive review. *Renewable and Sustainable Energy Reviews*, *155*, 111914. https://doi.org/10.1016/j.rser.2021.111914

Liem, M., & Jenny, P. (2020). Two-Stage Ensemble Kalman Filter Approach for Data Assimilation Applied to Flow in Fractured Media. *European Association of Geoscientists & Engineers*. https://doi.org/10.3997/2214-4609.202035126

Liem, M., Matthai, S. K., & Jenny, P. (2022). Estimation of Fracture Aperture in Naturally Fractured Reservoirs Using an Ensemble Smoother with Multiple Data Assimilation. *European Association of Geoscientists & Engineers*. https://doi.org/10.3997/2214-4609.202244068

Liu, G., Zhou, B., & Liao, S. (2018). Inverting methods for thermal reservoir evaluation of enhanced geothermal system. *Renewable and Sustainable Energy Reviews*, *82*, 471–476. https://doi.org/10.1016/j.rser.2017.09.065

Liu, J., Jiang, L., Liu, T., & Yang, D. (2023). Field-Scale Modeling of Interwell Tracer Flow Behavior to Characterize Complex Fracture Networks Based on the Embedded Discrete Fracture Model in a Naturally Fractured Reservoir. *SPE Journal*, *28*(03), 1062–1082. https://doi.org/10.2118/214297-PA

McLean, M. L., & Espinoza, D. N. (2023). Thermal destressing: Implications for short-circuiting in enhanced geothermal systems. *Renewable Energy*, *202*, 736–755. https://doi.org/10.1016/j.renene.2022.11.102

Olasolo, P., Juarez, M. C., Morales, M. P., D'Amico, S., & Liarte, I. A. (2016). Enhanced geothermal systems (EGS): A review. *Renewable and Sustainable Energy Reviews*, *56*, 133–144. https://doi.org/10.1016/j.rser.2015.11.031

Pandey, S. N., Chaudhuri, A., Kelkar, S., Sandeep, V. R., & Rajaram, H. (2014). Investigation of permeability alteration of fractured limestone reservoir due to geothermal heat extraction using three-dimensional thermo-hydro-chemical (THC) model. *Geothermics*, *51*, 46–62. https://doi.org/10.1016/j.geothermics.2013.11.004

Pandey, S. N., Vishal, V., & Chaudhuri, A. (2018). Geothermal reservoir modeling in a coupled thermo-hydro-mechanical-chemical approach: A review. *Earth-Science Reviews*, *185*, 1157–1169. https://doi.org/10.1016/j.earscirev.2018.09.004

Ping, J., & Zhang, D. (2013). History matching of fracture distributions by ensemble Kalman filter combined with vector based level set parameterization. *Journal of Petroleum Science and Engineering*, *108*, 288–303. https://doi.org/10.1016/j.petrol.2013.04.018

Pollack, A., & Mukerji, T. (2019). Accounting for subsurface uncertainty in enhanced geothermal systems to make more robust techno-economic decisions. *Applied Energy*, *254*, 113666. https://doi.org/10.1016/j.apenergy.2019.113666

Ranazzi, P. H., & Sampaio, M. A. (2019). Ensemble size investigation in adaptive ES-MDA reservoir history matching. *Journal of the Brazilian Society of Mechanical Sciences and Engineering*, *41*(10), 413. https://doi.org/10.1007/s40430-019-1935-0

Rawal, C., & Ghassemi, A. (2014). A reactive thermo-poroelastic analysis of water injection into an enhanced geothermal reservoir. *Geothermics*, *50*, 10–23. https://doi.org/10.1016/j.geothermics.2013.05.007

Ren, Y., Kong, Y., Pang, Z., & Wang, J. (2023). A comprehensive review of tracer tests in enhanced geothermal systems. *Renewable and Sustainable Energy Reviews*, *182*, 113393. https://doi.org/10.1016/j.rser.2023.113393

Ringel, L. M., Jalali, M., & Bayer, P. (2021). Stochastic Inversion of Three-Dimensional Discrete Fracture Network Structure With Hydraulic Tomography. *Water Resources Research*, *57*(12), e2021WR030401. https://doi.org/10.1029/2021WR030401

Salimzadeh, S., & Nick, H. M. (2019). A coupled model for reactive flow through deformable fractures in Enhanced Geothermal Systems. *Geothermics*, *81*, 88–100. https://doi.org/10.1016/j.geothermics.2019.04.010

Settgast, R. R., Fu, P., Walsh, S. D. C., White, J. A., Annavarapu, C., & Ryerson, F. J. (2017). A fully coupled method for massively parallel simulation of hydraulically driven fractures in 3-dimensions. *International Journal for Numerical and Analytical Methods in Geomechanics*, *41*(5), 627–653. https://doi.org/10.1002/nag.2557

Settgast, R. R., White, J. A., Corbett, B. C., Vargas, A., Sherman, C., Fu, P., & Annavarapu, C. (2018). GEOSX Simulation Framework, Version 00 [Software]. Retrieved from https://www.osti.gov/biblio/1422506

Shook, G. M., & Suzuki, A. (2017). Use of tracers and temperature to estimate fracture surface area for EGS reservoirs. *Geothermics*, *67*, 40–47. https://doi.org/10.1016/j.geothermics.2016.12.006

Somogyvári, M., Jalali, M., Jimenez Parras, S., & Bayer, P. (2017). Synthetic fracture network characterization with transdimensional inversion. *Water Resources Research*, *53*(6), 5104–5123. https://doi.org/10.1002/2016WR020293

Song, G., Song, X., Xu, F., Li, G., Shi, Y., & Ji, J. (2022). Contributions of thermo-poroelastic and chemical effects to the production of enhanced geothermal system based on thermo-hydro-mechanical-chemical modeling. *Journal of Cleaner Production*, *377*, 134471. https://doi.org/10.1016/j.jclepro.2022.134471

Tarrahi, M., Jafarpour, B., & Ghassemi, A. (2015). Integration of microseismic monitoring data into coupled flow and geomechanical models with ensemble Kalman filter. *Water Resources Research*, *51*(7), 5177–5197. https://doi.org/10.1002/2014WR016264

Tester, J. W., Anderson, B. J., Batchelor, A. S., Blackwell, D. D., DiPippo, R., Drake, E. M., et al. (2007). Impact of enhanced geothermal systems on US energy supply in the twenty-first century. *Philosophical Transactions of the Royal Society A: Mathematical, Physical and Engineering Sciences*, *365*(1853), 1057–1094. https://doi.org/10.1098/rsta.2006.1964

Todaro, V., D'Oria, M., Tanda, M. G., & Gómez-Hernández, J. J. (2022). genES-MDA: A generic open-source software package to solve inverse problems via the Ensemble Smoother with Multiple Data Assimilation. *Computers & Geosciences*, *167*, 105210. https://doi.org/10.1016/j.cageo.2022.105210

Vik, H. S., Salimzadeh, S., & Nick, H. M. (2018). Heat recovery from multiple-fracture enhanced geothermal systems: The effect of thermoelastic fracture interactions. *Renewable Energy*, *121*, 606–622. https://doi.org/10.1016/j.renene.2018.01.039

Vogt, C., Marquart, G., Kosack, C., Wolf, A., & Clauser, C. (2012). Estimating the permeability distribution and its uncertainty at the EGS demonstration reservoir Soultz-sous-Forêts using the ensemble Kalman filter. *Water Resources Research*, *48*(8). https://doi.org/10.1029/2011WR011673

Vu, M. T., & Jardani, A. (2022). Mapping discrete fracture networks using inversion of hydraulic tomography data with convolutional neural network: SegNet-Fracture. *Journal of Hydrology*, *609*, 127752. https://doi.org/10.1016/j.jhydrol.2022.127752

Witter, J. B., Trainor-Guitton, W. J., & Siler, D. L. (2019). Uncertainty and risk evaluation during the exploration stage of geothermal development: A review. *Geothermics*, *78*, 233–242. https://doi.org/10.1016/j.geothermics.2018.12.011

Wu, H., Fu, P., Hawkins, A. J., Tang, H., & Morris, J. P. (2021a). Predicting Thermal Performance of an Enhanced Geothermal System From Tracer Tests in a Data Assimilation Framework. *Water Resources Research*, *57*(12), e2021WR030987. https://doi.org/10.1029/2021WR030987

Wu, H., Fu, P., Morris, J. P., Mattson, E. D., Neupane, G., Smith, M. M., et al. (2021b). Characterization of flow and transport in a fracture network at the EGS Collab field experiment through stochastic modeling of tracer recovery. *Journal of Hydrology*, *593*, 125888. https://doi.org/10.1016/j.jhydrol.2020.125888

Wu, H., Fu, P., Yang, X., Morris, J. P., Johnson, T. C., Settgast, R. R., & Ryerson, F. J. (2019). Accurate imaging of hydraulic fractures using templated electrical resistivity tomography. *Geothermics*, *81*, 74–87. https://doi.org/10.1016/j.geothermics.2019.04.004

Xu, T., Ontoy, Y., Molling, P., Spycher, N., Parini, M., & Pruess, K. (2004). Reactive transport modeling of injection well scaling and acidizing at Tiwi field, Philippines. *Geothermics*, *33*(4), 477–491. https://doi.org/10.1016/j.geothermics.2003.09.012

Yasuhara, H., Kinoshita, N., Ohfuji, H., Lee, D. S., Nakashima, S., & Kishida, K. (2011). Temporal alteration of fracture permeability in granite under hydrothermal conditions and its interpretation by coupled chemo-mechanical model. *Applied Geochemistry*, *26*(12), 2074–2088. https://doi.org/10.1016/j.apgeochem.2011.07.005

Zhang, K., & Wu, H. (2023). Ensemble Smoother with Multiple Data Assimilation for Fracture Aperture Inversion from Tracer Tests [Software]. Zenodo. https://doi.org/10.5281/zenodo.10417269